NONCOHERENT COMMUNICATIONS USING SPACE-TIME TRELLIS CODES

A thesis

submitted in partial fulfilment

of the requirements for the degree of

Master of Engineering

in Electrical and Electronic Engineering

from the University of Canterbury

Christchurch, New Zealand

by

Yu Gu

University of Canterbury

June 2008

In philosophical discussions, we ought to step back from our senses, and consider things themselves, distinct from what are only perceptible measures of them.

Isaac Newton

This is dedicated to my father and all the fathers of the world. Their love has lighted the way for us in our darkest hours.

Abstract

In the last decade much interest has been shown in space-time trellis codes (STTCs) since they can offer coding gain along with the ability to exploit the space and time diversity of MIMO channels. STTCs can be flexibly designed by trading off performance versus complexity.

The work of Dayal [1] stated that if training symbols are used together with data symbols, then a space-time code can be viewed as a noncoherent code. The authors of [1] described the migration from coherent space-time codes to training assisted noncoherent space-time codes.

This work focuses on the development of training assisted noncoherent STTCs, thus extending the concept of noncoherent training codes to STTCs. We investigate the intrinsic link between coherent and noncoherent demodulation. By analyzing noncoherent STTCs for up to four transmit antennas, we see that they have similar performance deterioration to noncoherently demodulated M-PSK using a single antenna. Various simulations have been done to confirm the analysis.

Acknowledgements

First and foremost, I would like to thank my supervisor Professor Desmond Taylor and co-supervisor Dr. Philippa Martin for their long time guidance and support during my master's research. Without their instructive advice and tireless help, my thesis work would not have been completed.

My acknowledgements also go to the communication group of U.C. I would like to thank Dr. Peter Green, Yao-Hee Kho, Rui Lin, Michael Krause and Gayathri Kongara for their valuable discussions.

My special thanks go to my parents who taught me to say the first word and taught me to write the first letter in my life. Their encouragement and emotional support made my life full of warm and unforgettable moments.

Yu Gu

June 2008

Contents

List of Figures

List of Tables

Chapter 1

Introduction

1.1 Introduction

In the past 20 years, wireless communication has evolved from analog, single medium (voice), and low data rate (a few kilobits per second) systems to the digital, multimedia, and high data rate (ten to hundreds of megabits per second) systems of today. Future wireless communication systems may require high spectral efficiency and flexible inter-operability across heterogeneous networks to provide personalized and integrated services to users [5]. Many of the envisaged applications will require high data rates.

The International Telecommunication Union (ITU) has formulated a recommendation regarding the direction of future technological developments including fourth generation (4G) communication systems [6]. 4G systems are expected to support data rates in the order of 100 Mbits/s in the outdoor environment and 1 Gbits/s in the indoor environment [7]. Any proposed system that can meet these requirements with lower bandwidth will be considered. There are various competing wireless communication technologies that may be used. In order to support the required large throughputs, wireless communication systems must employ signalling formats and receiver algorithms that provide a significant increase in spectrum efficiency and capacity over cur-

rent systems. Recently, a lot of research on multiple-input multiple-output (MIMO) systems has been performed [8, 4, 9, 10]. This has occurred due to the potential for MIMO systems to provide a linear increase in capacity and throughput with antenna numbers [11]. In order to exploit diversity at the transmit and receive antennas, MIMO architectures are used to provide multiple data transmission paths. The number of inputs and outputs refers to the number of antennas used at the transmitter and receiver, respectively.

1.2 Wireless Communication Systems

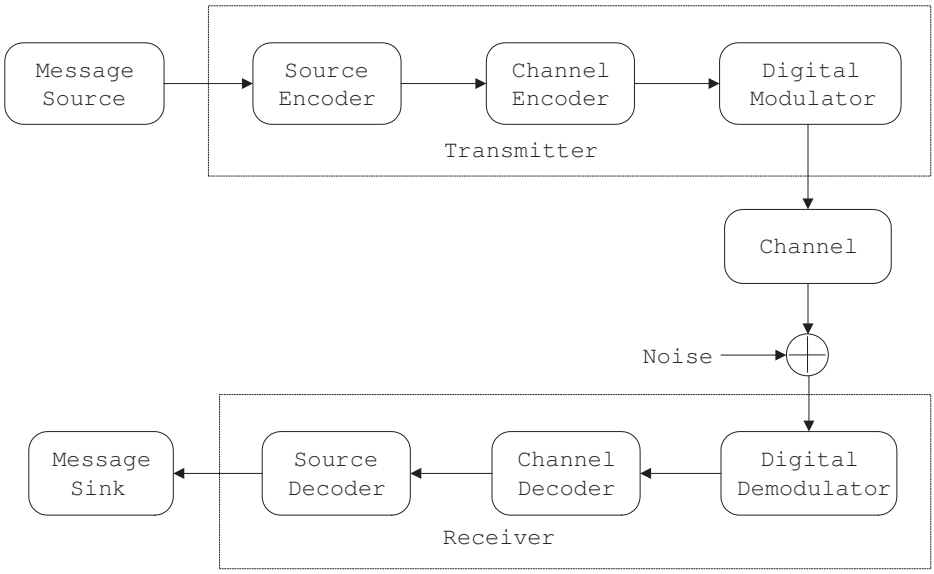

Figure 1.1: Block diagram of a wireless communication system.

A block diagram showing signal flow through a typical communications system is illustrated in Figure 1.1. In a digital communication system, the message source typically generates a sequence of binary data. It may consist of digital samples of analog inputs such as audio and video, and purely digital sources (computer data). For most systems, limited bandwidth is either a physical or regulatory constraint.

The efficient representation of the source output is often achieved through source encoding or data compression. The source encoded sequences are then delivered to the channel encoder for further processing. As the compressed information sequences are susceptible to channel interference, redundancy is deliberately added by the channel encoder to help overcome undesirable effects due to the communication channel and the additive noise.

The digital modulator maps the digital information sequences to corresponding analog radio waveforms. In baseband representation, information sequences are mapped to a complex signal constellation and then transmitted from either a single antenna or multiple antennas. The information source, source encoder, channel encoder and modulator are collectively known as the transmitter.

The physical medium over which the signals are transferred from the transmitter to the receiver is known as the channel. An ideal channel has no fading or other channel perturbations. The only concern for the receiver operating on an ideal channel is the disturbance caused by the presence of thermal noise primarily due to the receiver amplifier. The thermal base band noise is modelled as additive white Gaussian noise (AWGN) [12].

In a wireless communication system, the channel is usually more complicated than the simple AWGN model. For example, the fixed-access line of sight digital microwave radio channel is a multi-path fading channel [13]. In such a channel, the received signal is the linear combination of components arriving via multiple channel paths reflected by obstacles such as trees, cars, buildings or atmospheric disturbance [12]. If multiple transmit antennas and receive antennas are used (a MIMO channel model is used), the reflected radio signals typically travel over several uncorrelated propagation paths and arrive at different receive antennas with different phases and signal levels.

A quasi-static Rayleigh fading MIMO channel is used in this thesis. It is a multi-path channel corresponding to slow fading conditions.

The digital demodulator recovers the data sequence from received signals. The demodulated sequences are then sent to the channel decoder to reconstruct the original data streams. The original message sequences are then reconstructed from these sequences using the source decoder. These elements are collectively known as the receiver.

The fundamental objective of communication system design is the effective delivery of information from transmitter to receiver with acceptable number of errors dependent on the application.

1.3 From Hamming Code to Alamouti Code

The history of forward error correction (FEC) or channel coding dates back to Shannon's pioneering work [14] in 1948. It predicts that arbitrarily reliable communications is achievable by adding redundant information to the transmitted messages. However, Shannon did not propose explicit coding schemes for implementation.

The single error-correcting Hamming code [15] was one of the first practical FEC codes and was proposed in 1950. The Hamming block code is not powerful enough for most practical applications. A family of important and powerful block codes, Bose-Chaudhuri-Hocquenghem (BCH) codes were discovered in 1959 [16] and 1960 [17, 18]. It was later recognized that these codes exhibit a cyclic structure, meaning all cyclically shifted versions of a legitimate codeword are also legitimate codewords [19]. In 1960, Reed-Solomon (RS) codes were discovered [20]. They are non-binary subset of BCH codes. The block lengths and symbol sizes of BCH and RS codes can be adjusted to accommodate the message sizes. They provide a range of code rates that

can be chosen to satisfy performance requirements. In recent years, RS codes have found many practical applications such as in compact disc players and deep-space communications [21].

Convolutional codes were discovered in 1955 by Elias [22]. Various decoding algorithms for them have been proposed by Wozencraft and Reiffen [23, 24], Fano [25] and Massey [26]. Among the efforts to find an effective decoder structure, the Viterbi algorithm (VA) [27] for maximum likelihood sequence estimation (MLSE) was a milestone in the implementation of convolutional error correcting codes. A detailed tutorial interpretation of the VA can be found in Forney's frequently cited paper [28]. The VA finds the most likely transmitted information sequence. One of the first practical applications of convolutional codes that utilized the VA as a decoder was developed by Heller and Jacobs during the seventies [29]. From the early 1970s, error correcting codes were incorporated into various satellite communication systems, such as in the Anik domestic satellite system in Canada [13].

Coding and modulation were treated as distinct subjects in communications from the 1970s. By integrating coding and modulation, and using an enlarged signal set, Ungerboeck developed trellis-coded modulation (TCM) [30, 31]. The redundant and information bits impose certain patterns on the transmitted signal set. The *set partitioning* approach used to design these codes involves partitioning a constellation successively into smaller subsets with progressively increasing minimum Euclidean distance between their respective signal points. TCM achieves significant coding gains without increasing bandwidth by using an enlarged signal constellation.

A historic breakthrough in error control coding was the invention of turbo codes by Berrou *et al.* in 1993 [32]. These codes can push the operation of communication systems close to the Shannon capacity limit. Turbo coding is

based on a composite code consisting of two recursive convolutional encoders and an interleaver.

1.4 Multiple-input Multiple-output Systems

Modern mobile communication systems are expected to provide users with a wide range of services at high data rates. To support these rates, the throughput of band-limited wireless channels can be increased by employing multiple antennas to achieve diversity. Classically, this involves multiple antennas at the receiver and maximum ratio combining (MRC) [33, 34, 35] of the received signals to improve performance. This single-input multiple-output (SIMO) architecture collects more energy, which improves the signal-to-noise ratio (SNR).

Signal power in a wireless channel fluctuates with time and space. When the received signal power drops dramatically, the channel is said to fade. Diversity is used in wireless systems to combat fading. The principle of antenna diversity is to provide the receiver with several independently faded versions of the transmitted signal. As the number of diversity branches increases, the probability that at any instant of time, one or more branches is not in a fade increases. Thus diversity helps to stabilize a wireless link.

Space-time codes (STCs) are designed to achieve transmit diversity. A wireless system using a STC encodes and modulates the information sequence, and conveys it over multiple transmit antennas to one or more receive antennas thereby creating a multiple-input single-output (MISO) or MIMO channel. The received signals are demodulated and decoded accordingly. The STCs fall into two main categories: STBCs and STTCs.

Driven by the desire to support high data rates for a wide range of bearer services, Tarokh *et al.* proposed space-time trellis codes (STTCs) in 1998

[4]. STTCs can provide high throughput on band-limited wireless channels through jointly designing the coding and modulation for multiple transmit antennas. Later, Alamouti introduced a low-complexity space-time block code (STBC) that offers significantly lower complexity at the cost of a slight degradation in performance [8]. This Alamouti code motivated Tarokh *et al.* to generalize Alamouti's scheme to an arbitrary number of transmit antennas [36].

1.4.1 Space-Time Block Codes

Orthogonal STBCs are essentially modulation schemes for multiple transmit antennas. They provide transmit diversity, but no coding gain. The best-known STBC is the Alamouti code for two transmit antennas and one or more receive antennas [8]. The generator matrix of the Alamouti code is given by

$$G = \begin{pmatrix} x_1 & x_2 \\ -x_2^* & x_1^* \end{pmatrix} \tag{1.1}$$

where each row corresponds to a different time slot and each column to a different transmit antenna. This can be viewed as a repetition code over space and time, simultaneously transmitting the same data over multiple antennas. The information is transmitted over different paths to mitigate fading. Diversity gain is achieved by transmitting an independent replica of the required information. To obtain good spectral efficiency, a high order modulation must be used, giving tighter constraints on the linearity of radio frequency (RF) amplifiers and analog-to-digital converter (ADC) / digital-to-analog converter (DAC) resolution. Thus, the main objective of STBCs is not to increase the data rate, but to improve the robustness of the wireless link [37].

No full rate (rate 1) complex orthogonal STBC exists with more than two transmit antennas, $n_T > 2$ [36]. Note rate is defined as the number of transmitted data symbols per time interval regardless of n_T. When four transmit antennas are used, $n_T = 4$, orthogonal STBCs can convey at most three information symbols within four symbol time intervals, and thus incur a rate loss (rate 3/4). Some quasi-orthogonal STBCs with full rate do exist [38], but they have higher decoding complexity than orthogonal STBCs.

Optimal decoding of orthogonal STBCs is relatively simple compared to STTCs since only linear processing is required [39]. The complexity of STBCs increases linearly with the number of transmit antennas. In mobile wireless communication systems, the mobile transceiver has limited battery power and computational capacity. Therefore, low complexity STBCs are desirable. They enjoy popularity in wireless cellular standards such as Universal Mobile Telecommunications System (UMTS) and wireless networking standards such as IEEE 802.11n and IEEE 802.16e [37].

1.4.2 Space-Time Trellis Codes

STTCs combine modulation and convolutional coding to transmit information using multiple transmit antennas over a MIMO channel. This scheme transmits information and redundant symbols distributed over both time and a set of transmit antennas. Therefore, correlation in both the temporal and spatial dimensions is achieved. The receiver typically performs MLSE, using the VA, to decode the received signals [4].

In contrast to STBCs, STTCs are able to provide both coding gain and diversity gain. STTCs can show considerable performance gain for wireless communication at the expense of a rising decoding effort with increasing numbers of transmit antennas or trellis states.

The complexity of STTCs increases exponentially with the number of transmit antennas and the size of the signal constellation [4]. The number of trellis encoder and decoder states has to be very large for STTCs to achieve full diversity for a large number of transmit antennas. This results in large computational effort and memory storage. For example, 64 and 1024 states is the minimum requirement for a QPSK STTC with four and six transmit antennas, respectively. This also makes maximum-likelihood (ML) decoding at the receiver very complicated. To address this issue, the combination of transmit antenna selection and STTCs for a small number of transmit antennas can be used [40].

1.4.3 MIMO Channel Capacity

The best possible system performance is called channel capacity. It was defined for the AWGN channel by Shannon in [14]. It states that an arbitrarily small probability of error can be achieved at all rates less than capacity. The expression of channel capacity for multiple transmit antenna systems in the presence of fading and Gaussian noise was first derived in [41], which was later published in [42]. The fading is assumed to be independent from one channel to another. In [11], the capacity of a multi-antenna system on a quasi-static fading channel was derived. The quasi-static fading channel is constant for a given period of time and then changes in an independent manner. The channel capacity in [11] is given by

$$C = B \log_2 \left| \mathbf{I} + \frac{SNR}{n_T} \mathbf{H}\ \mathbf{H}^* \right| \quad bits/s \tag{1.2}$$

where $\mathbf{H}$ is an $n_R \times n_T$ channel matrix, $\mathbf{I}$ is an $n_R \times n_R$ identity matrix and n_R denotes the number of receive antennas. SNR denotes the signal-to-noise ratio per receive antenna and B denotes the bandwidth of the channels.

The channel capacity of (1.2) provides a bound on the maximum achievable information rate in a MIMO channel.

For a single transmit and single receive antenna system, the channel matrix **H** reduces to a scalar. Therefore, (1.2) can be simplified to the Shannon information capacity, which is given by [43, 44]

$$C = B \log_2 (1 + SNR) \quad bits/s. \tag{1.3}$$

It defines the maximum rate at which information can be transmitted across a single channel without error. It can be seen from (1.2) and (1.3) that the dependence of channel capacity C on bandwidth B is linear, whereas its dependence on SNR is logarithmic. Accordingly, it is easier to increase the channel capacity by expanding bandwidth rather than increasing the transmitted power for a prescribed noise variance.

1.5 Motivation and Objectives

The high capacity and high spectral efficiency offered by MIMO technology has made it an attractive technique for wireless systems. It could be used in a number of wireless environments. Coherent detection requires an accurate phase reference and complete channel state information (CSI). When the channel coherence time is short and it is not possible to obtain complete CSI, differential detection is often used to demodulate received signals over time varying channels.

The objective of this thesis is to develop non-differential STTC systems for noncoherent communication and to investigate their performance in fading channels. This thesis

- Presents a survey of MIMO and space-time coding technologies including STTCs.

- Investigates the key requirements for designing spectrally efficient STTCs on MIMO channel by applying appropriate design criteria for the number of transmit antennas.
- Summarizes the decoding of STTCs using the VA.
- Investigates the relationship between coherent and noncoherent modulation, and proposes STTCs using training assistance [1] .
- Provides detailed performance analysis of noncoherent STTCs when two and four transmit antennas are used.
- Presents the performance of noncoherent STTCs for various numbers of transmit antenna, channel modelling, and number of training symbols.

1.6 Organization of Thesis

The thesis is divided into five chapters. The first part, Chapter 1 and Chapter 2, provides a review of MIMO technology, STBCs and STTCs. The second part, Chapters three, four and five, provides detailed development, design, analysis and simulation of the training-assisted STTCs for noncoherent communication.

Chapter 2 describes how to encode STTCs and how to decode them using the VA. A STTC encoder example is given for illustration. By applying appropriate space-time code design criteria, optimum space-time trellis coded schemes for various numbers of transmit antennas and spectral efficiencies are constructed.

Chapter 3 begins by reviewing existing noncoherent STCs for wireless communications. This chapter shows the inherent relationship between coherent and noncoherent modulation by analyzing a differential demodulator when a single transmit antenna is used. It demonstrates that differential detection actually extracts CSI from the previous symbol. Based on the

concept of using pilot symbols for noncoherent MIMO communication [45], we use pilot symbols with the STTCs in each frame. Analysis shows that the performance of the noncoherent STTCs is around 3 dB inferior to the coherent STTCs.

Chapter 4 describes the simulation setup and results. It starts by defining the simulation environment. Performance of the coherent and noncoherent STTCs are simulated over quasi-static channels. The simulation results show that the performance gap between the coherent and noncoherent STTCs is approximately 3 dB. The performance of the noncoherent STTCs can be improved under some conditions by using more training symbols. This chapter also shows the performance of noncoherent STTCs on a continuously varying Rayleigh fading channel, and shows good performance when the normalized Doppler spread is small. The performance starts to degrade when the normalized Doppler spread increases.

Chapter 5 summarizes the ideas presented in this thesis. The advantages and limitations of the proposed noncoherent STTCs are also discussed. Finally a brief discussion of possible future work relating to noncoherent STTCs is presented.

1.7 Summary

This chapter has provided a brief review of MIMO technology along with space-time coding techniques. The major features of the technology were explained and some of the advantages were discussed. Two of the most important forms of STCs, namely STBCs and STTCs, were presented and compared. Finally the scope and organization of the thesis were summarized.

Chapter 2

Space-Time Trellis Codes

2.1 Introduction

Space-time trellis codes (STTCs) have attracted considerable interest for high data rate wireless communications. They can provide significant diversity gain as well as the coding gain that can not be provided by space-time block codes (STBCs). STTCs can be designed as full-rate codes (one data symbol per time slot), so that they do not introduce bandwidth expansion.

STTCs were introduced by Tarokh, Seshadri and Calderbank [4] in 1998. This caused the development [3, 46, 2, 9, 47] of design criteria for various conditions. Better codes in specific conditions were obtained through complete generater coefficient searches according to the rank and determinant criteria [4], and the trace criterion [47].

In this chapter, we describe the system model and encoder structure of STTCs. By applying the STTC design criteria [4, 47], good STTCs for various numbers of transmit and receive antennas are constructed and compared. We also describe the Viterbi algorithm (VA), which is used for decoding.

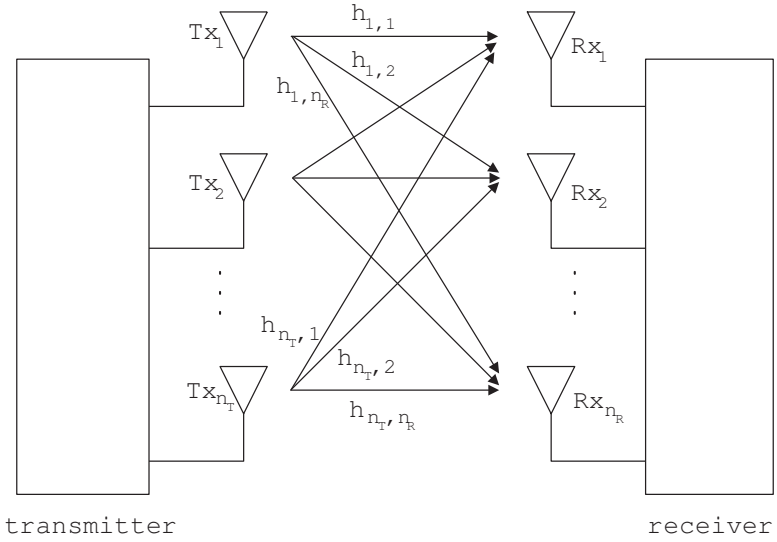

Figure 2.1: A MIMO system model.

2.2 System Model

We consider a communication system where the transmitter is equipped with n_T antennas, and the receiver is equipped with n_R antennas. The channel is modelled by a $n_T \times n_R$ matrix, denoted by $\mathbf{H}$. The elements of $\mathbf{H}$, denoted by $h_{i,j}, 1 < i \leq n_T, 1 \leq j \leq n_R$, are fading coefficients or channel gains between the ith transmit antenna and the jth receive antenna. The system model is shown in Figure 2.1. In any time slot, t, the output of the ith transmit antenna is a complex symbol $x_{i,t}, i = 1, 2, ..., n_T$. The signal received at the jth receive antenna, $1 \leq j \leq n_R$, at time t is then given by [4]

$$r_{j,t} = \sum_{i=1}^{n_T} h_{i,j} x_{i,t} + n_{j,t} \tag{2.1}$$

where the noise at time t, $n_{j,t}$, is modelled as independent samples of additive white Gaussian noise (AWGN) with one sided power spectral density N_o.

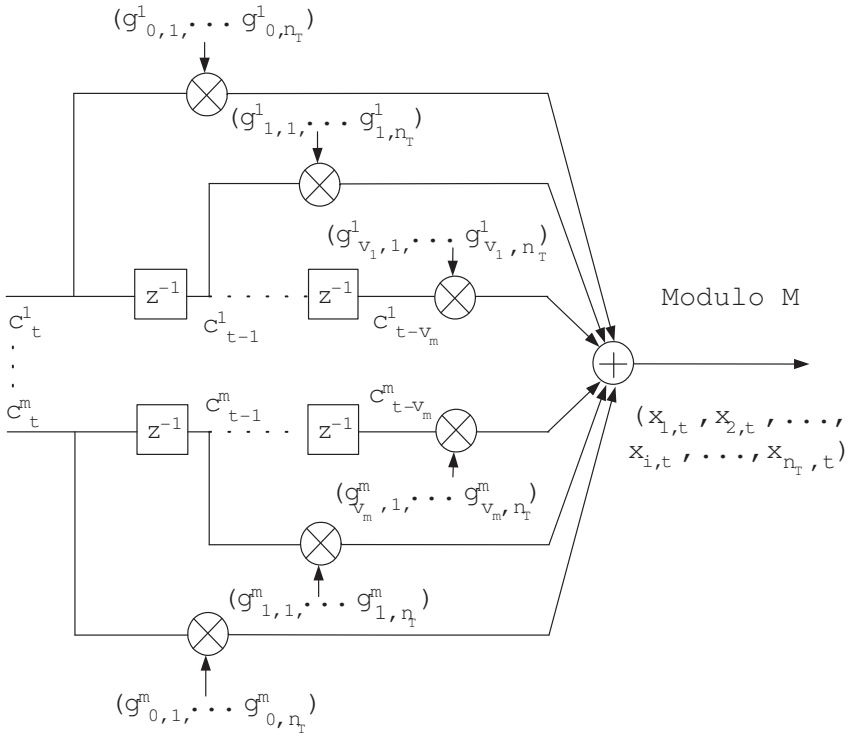

Figure 2.2: STTC encoder structure [2].

2.3 STTC Encoder

In [2], the authors describe a general encoder structure for STTCs using multiple transmit antennas. The binary inputs to the encoder are mapped by generator coefficients to modulation symbols. The encoding process can be described by a trellis diagram.

The encoder structure of a STTC with n_T transmit antennas using M-ary phase shift keying (M-PSK) is shown in Figure 2.2. The input message codeword is denoted $\mathbf{c} = (\mathbf{c}_0, \mathbf{c}_1, \mathbf{c}_2, ..., \mathbf{c}_t, ...)$, where $\mathbf{c}_t = (c_t^1, c_t^2, ..., c_t^m)$ denotes the $m = log_2 M$ information bits at time t. A one-bit delay in a shift register is denoted z^{-1}.

In the STTC encoder, binary input sequences are fed into the m shift

registers. The kth input sequence is passed into the kth feedforward shift register, where $k = 1, 2, ..., m$. It is then multiplied by an encoder coefficient sequence. The outputs from all multipliers are added modulo M, giving the encoder output $\mathbf{x}_t = (x_{1,t}, x_{2,t}, ..., x_{n_T,t})$. The multiplication coefficients of the modulo M multipliers can be written as [2]

$$\mathbf{g}^1 = [(g^1_{0,1}, g^1_{0,2}, ..., g^1_{0,n_T}), (g^1_{1,1}, g^1_{1,2}, ..., g^1_{1,n_T}), ..., (g^1_{v_1,1}, g^1_{v_1,2}, ..., g^1_{v_1,n_T})] \quad (2.2)$$

$$\mathbf{g}^2 = [(g^2_{0,1}, g^2_{0,2}, ..., g^2_{0,n_T}), (g^2_{1,1}, g^2_{1,2}, ..., g^2_{1,n_T}), ..., (g^2_{v_2,1}, g^2_{v_2,2}, ..., g^2_{v_2,n_T})] \quad (2.3)$$

$$\vdots$$

$$\mathbf{g}^k = [(g^k_{0,1}, g^k_{0,2}, ..., g^k_{0,n_T}), (g^k_{1,1}, g^k_{1,2}, ..., g^k_{1,n_T}), ..., (g^k_{v_k,1}, g^k_{v_k,2}, ..., g^k_{v_k,n_T})] \quad (2.4)$$

$$\vdots$$

$$\mathbf{g}^m = [(g^m_{0,1}, g^m_{0,2}, ..., g^m_{0,n_T}), (g^m_{1,1}, g^m_{1,2}, ..., g^m_{1,n_T}), ..., (g^m_{v_m,1}, g^m_{v_m,2}, ..., g^m_{v_m,n_T})] \quad (2.5)$$

where $g^k_{j,i}, k = 1, 2, ..., m, j = 1, 2, ..., v_k, i = 1, 2, ..., n_T$, is an element of the M-PSK constellation set, and v_k is the memory order of the kth shift register. The sets of multiplication coefficients are also called the generator sequences [48].

The encoder maps the input sequence, $\mathbf{c}$, into an M-PSK modulated signal sequence. The encoder output at time t for transmit antenna i is given by [2]

$$x_{i,t} = \sum_{k=1}^{m} \sum_{j=0}^{v_k} g^k_{j,i} c^k_{t-j} \quad (modulo \quad M). \quad (2.6)$$

The modulated signals are transmitted simultaneously by n_T transmit antennas. The transmitted signal vector at time t is given by $\mathbf{x}_t = (x_{1,t}, x_{2,t}, ..., x_{n_T,t})$, where the encoder outputs, $\mathbf{x}$, are M-PSK symbols. Most M-PSK STTCs achieve a bandwidth efficiency of m bits/s/Hz. The total memory order of the decoder is given by [48]

$$v = \sum_{k=1}^{m} v_k. \quad (2.7)$$

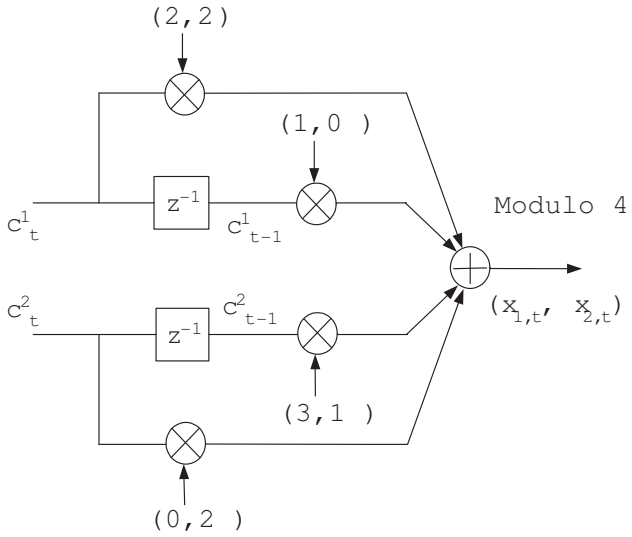

Figure 2.3: Four-state STTC encoder for two transmit antennas.

The value of v_k for M-PSK constellations is determined by

$$v_k = \left\lfloor \frac{v + k - 1}{\log_2 M} \right\rfloor, \tag{2.8}$$

where $\lfloor a \rfloor$ denotes the largest integer $\leq a$. The total number of states for the trellis encoder is 2^v.

2.3.1 An Encoder Example

In this section, we give a simple example of a four-state STTC encoder using QPSK and two transmit antennas as shown in Figure 2.3. The encoder's generator sequences are given by [3]

$$\mathbf{g^1} = [(2,2),(1,0)], \tag{2.9}$$

$$\mathbf{g^2} = [(0,2),(3,1)]. \tag{2.10}$$

The trellis consists of $2^v = 4$ states corresponding to the contents of the 2 shift registers. The trellis description of the generator is shown in Figure 2.4. The

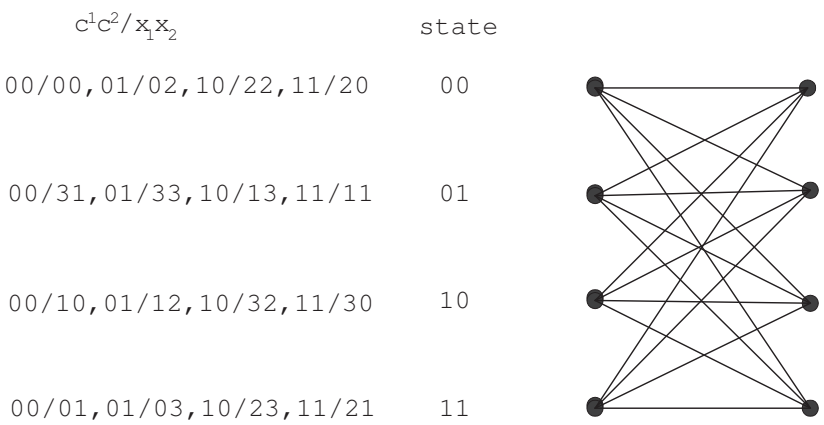

Figure 2.4: Trellis of a four-state STTC using QPSK system and two transmit antennas [3].

encoder accepts $m = 2$ input bits at each time. There are $2^m = 4$ branches leaving each state corresponding to four different input combinations. Each branch is labelled by $c_t^1 c_t^2 / x_{1,t} x_{2,t}$, where $c_t^1 c_t^2$ are a pair of encoder input bits, and $x_{1,t} x_{2,t}$ are the two coded QPSK symbols transmitted through antennas one and two at time, t, respectively. Transitions from each state node, with the associated output QPSK symbols $x_{1,t} x_{2,t}$, are uniquely decided by the encoder inputs $c_t^1 c_t^2$. Let us assume an input sequence

$$\mathbf{c} = (11, 10, 01, 10). \tag{2.11}$$

The space-time trellis encoder generates output sequences for antenna one and antenna two respectively, which are defined by

$$x_{1,t} = 2c_t^1 + c_{t-1}^1 + 0c_t^2 + 3c_{t-1}^2 \qquad (modulo \quad 4) \tag{2.12}$$

$$x_{2,t} = 2c_t^1 + 0c_{t-1}^1 + 2c_t^2 + c_{t-1}^2 \qquad (modulo \quad 4). \tag{2.13}$$

The QPSK signals from the 1st to 4th symbol times after complex signal constellation mapping, for antennas one and two respectively, are

$$\mathbf{x_1} = \left[\exp\left(2 \cdot \frac{\pi j}{2}\right), \exp\left(0 \cdot \frac{\pi j}{2}\right)\right] \tag{2.14}$$

$$\mathbf{x_3} = \left[\exp\left(2 \cdot \frac{\pi j}{2}\right), \exp\left(3 \cdot \frac{\pi j}{2}\right)\right] \tag{2.15}$$

$$\mathbf{x_3} = \left[\exp\left(1 \cdot \frac{\pi j}{2}\right), \exp\left(2 \cdot \frac{\pi j}{2}\right)\right] \tag{2.16}$$

$$\mathbf{x_4} = \left[\exp\left(1 \cdot \frac{\pi j}{2}\right), \exp\left(3 \cdot \frac{\pi j}{2}\right)\right], \tag{2.17}$$

where j is defined as $\sqrt{-1}$. The resulting QPSK signal squences are ready for transmission.

2.4 Code Design Criteria for Small Values of rn_R

Tarokh *et al.* derived performance criteria for designing STTCs under the assumption that the fading is slow and frequency nonselective [4]. They are known as the rank and determinant criteria for flat Rayleigh fading channels. Chen *et al.* pointed out that they are best applied for small values of rn_R, where r is the rank of the STTC distance matrix [2]. The rank and determinant criteria are now summarized based on [2].

A wireless communication system with n_T transmit and n_R receive antennas is considered. Assume that the encoded signal sequence

$$\mathbf{x} = (x_{1,1}x_{2,1}...x_{n_T,1}, x_{1,2}x_{2,2}...x_{n_T,2}, ..., x_{1,t}x_{2,t}...x_{n_T,t}, ..., x_{1,l}x_{2,l}...x_{n_T,l}) \tag{2.18}$$

was transmitted, where l is codeword length. A maximum-likelihood receiver might decide erroneously in favor of another codeword, say

$$\mathbf{e} = (e_{1,1}e_{2,1}...e_{n_T,1}, e_{1,2}e_{2,2}...e_{n_T,2}, ..., e_{1,t}e_{2,t}...e_{n_T,t}, ..., e_{1,l}e_{2,l}...e_{n_T,l}). \tag{2.19}$$

The difference matrix $\mathbf{B}(\mathbf{x}, \mathbf{e})$ is a $n_T \times l$ matrix, which is defined as

$$\mathbf{B}(\mathbf{x},\mathbf{e}) = \begin{pmatrix} e_{1,1}-x_{1,1} & \dots & e_{1,t}-x_{1,t}\dots & e_{1,l}-x_{1,l} \\ \vdots & \ddots & \vdots & \ddots & \vdots \\ e_{n_T,1}-x_{n_T,1}\dots & e_{n_T,t}-x_{n_T,t}\dots & e_{n_T,l}-x_{n_T,l} \end{pmatrix}. \quad (2.20)$$

We can construct an $n_T \times n_T$ squared distance matrix, $\mathbf{A}(\mathbf{x},\mathbf{e})$, which is defined as

$$\mathbf{A}(\mathbf{x},\mathbf{e}) = \mathbf{B}(\mathbf{x},\mathbf{e})\mathbf{B}^*(\mathbf{x},\mathbf{e}) \quad (2.21)$$

where $\mathbf{B}^*(\mathbf{x},\mathbf{e})$ denotes the transposed conjugate of $\mathbf{B(x,e)}$. The conditional pairwise error probability then has the upper bound [4]

$$P(\mathbf{x}\to\mathbf{e}|\mathbf{H}) \le \frac{1}{2}\exp\left[\frac{-d^2(\mathbf{x},\mathbf{e})E_s}{4N_o}\right] \quad (2.22)$$

where $d^2(\mathbf{x},\mathbf{e})$ is the codeword distance given by

$$\begin{aligned} d^2(\mathbf{x},\mathbf{e}) &= tr\{\mathbf{HB}(\mathbf{x},\mathbf{e})[\mathbf{HB}(\mathbf{x},\mathbf{e})]^*\} \quad (2.23)\\ &= \sum_{t=1}^{l}\sum_{j=1}^{n_R}\left|\sum_{i=1}^{n_T} h_{i,j}(x_{i,t}-e_{i,t})\right|^2, \end{aligned}$$

E_s is the energy per symbol at each transmit antenna and $tr(\cdot)$ denotes the trace of a matrix. The conditional pairwise error probability of (2.23) can also be written as [4]

$$P(\mathbf{x}\to\mathbf{e}|\mathbf{H}) \le \left[\frac{1}{\prod_{i=1}^{n_T}(1+\lambda_i\frac{E_s}{4N_o})}\right]^{n_R}. \quad (2.24)$$

When the SNR is high, this upper bound can be simplified to

$$P(\mathbf{x}\to\mathbf{e}|\mathbf{H}) \le \left(\prod_{i=1}^{r}\lambda_i\right)^{-n_R}\left(\frac{E_s}{4N_o}\right)^{-rn_R} \quad (2.25)$$

where $\lambda_1\lambda_2...\lambda_i$ are the nonzero eigenvalues of the matrix $\mathbf{A}(\mathbf{x},\mathbf{e})$.

codes	n_T	states	generator sequence	rank	det
Tarokh *et al.*'s	2	4	$\mathbf{g^1} = [(0,2),(2,0)]$ $\mathbf{g^2} = [(0,1),(1,0)]$	2	4.0
Bäro *et al.*'s	2	4	$\mathbf{g^1} = [(2,2),(1,0)]$ $\mathbf{g^2} = [(0,2),(3,1)]$	2	8.0
Tarokh *et al.*'s	2	8	$\mathbf{g^1} = [(0,2),(2,0)]$ $\mathbf{g^2} = [(0,1),(1,0),(2,2)]$	2	12.0
Bäro *et al.*'s	2	8	$\mathbf{g^1} = [(2,2),(1,0)]$ $\mathbf{g^2} = [(0,2),(3,1),(2,2)]$	2	12.0
Tarokh *et al.*'s	2	16	$\mathbf{g^1} = [(0,2),(2,0),(0,2)]$ $\mathbf{g^2} = [(0,1),(1,2),(2,0)]$	2	12.0
Bäro *et al.*'s	2	16	$\mathbf{g^1} = [(0,2),(2,0),(0,2)]$ $\mathbf{g^2} = [(2,1),(1,2),(2,0)]$	2	20.0

Table 2.1: Two transmit antenna QPSK STTCs based on the determinant and rank criteria [3, 4].

In order to minimize the pairwise error probability of (2.25), both rn_R and $\prod_{i=1}^{r} \lambda_i$ must be maximized. The diversity order is given by rn_R. It is determined by the minimum rank, r, of the matrix $\mathbf{A}(\mathbf{x}, \mathbf{e})$ over all codeword pairs $(\mathbf{x}, \mathbf{e})$ and the number of receive antennas. The minimum rank of $\mathbf{A}(\mathbf{x}, \mathbf{e})$ is also referred to as the rank of the STTC. The coding gain is given by $(\lambda_1 \cdot \lambda_2 \cdot ... \cdot \lambda_r)^{\frac{1}{r}}$. Maximizing coding gain is equivalent to maximizing the determinant of $\mathbf{A}(\mathbf{x}, \mathbf{e})$ over all codeword pairs $(\mathbf{x}, \mathbf{e})$.

2.5 STTCs Based on the Rank and Determinant Criteria

Tarokh *et al.* heuristically designed some STTCs and showed some performance curves for the Rayleigh flat fading channel [4]. The simulation results show that as the number of trellis states increases, the coding gain of the

system increases. However, STTCs for a given encoder complexity do not necessarily achieve maximum coding gain since they may not be designed according to any particular design criterion.

Bäro *et al.* introduced several new STTCs and presented results of a systematic code search [3] according to the design criteria developed in [4]. The search produced STTCs that perform better than those in [4] at the same complexity. In Table 2.1, Tarokh *et al.*'s codes and Bäro *et al.*'s codes for two transmit antennas and QPSK are listed. It should be noted that determinants of the systematically searched Bäro *et al.*'s codes are at least as large as that of the Tarokh *et al.*'s codes. Therefore, the STTCs of [3] have good coding gain if the number of transmit antennas is small.

2.6 Code Design Criteria for Large Values of rn_R

Chen *et al.* developed a criterion for designing STTCs [2] based on the assumption that the system has a large diversity order. Full rank $r = n_T$ is not always achievable due to restrictions imposed by the code trellis. The maximum rank of a STTC is $\min(n_T, \lfloor \frac{\nu}{2} \rfloor + 1)$ [2]. They found that if the diversity order is larger than or equal to three, the so-called trace or Euclidean distance criterion should be used. Their derivation is summarized in the following, based on the description in [9] and [2].

We write the codeword distance (2.23) as

$$\begin{aligned} d^2(\mathbf{x}, \mathbf{e}) &= tr\{\mathbf{HB}(\mathbf{x}, \mathbf{e})[\mathbf{HB}(\mathbf{x}, \mathbf{e})]^*\} \\ &= tr[\mathbf{HB}(\mathbf{x}, \mathbf{e})\mathbf{B}^*(\mathbf{x}, \mathbf{e})\mathbf{H}^*] \end{aligned} \tag{2.26}$$

By using the cyclic property of trace which allows cyclic permutation of

matrices [49], we can rewrite (2.26) as

$$\begin{aligned} d^2(\mathbf{x},\mathbf{e}) &= tr\left[\mathbf{B}^*(\mathbf{x},\mathbf{e})\mathbf{H}^*\mathbf{H}\mathbf{B}(\mathbf{x},\mathbf{e})\right] \\ &= tr\left[n_R\mathbf{B}^*(\mathbf{x},\mathbf{e})\frac{\mathbf{H}^*\mathbf{H}}{n_R}\mathbf{B}(\mathbf{x},\mathbf{e})\right]. \end{aligned} \tag{2.27}$$

Let

$$\mathbf{M} = \frac{\mathbf{H}^*\mathbf{H}}{n_R} \tag{2.28}$$

with elements

$$m_{i,j} = \frac{1}{n_R}\sum_{k=1}^{n_R}\bar{h}_{i,k}h_{j,k} \tag{2.29}$$

where $\bar{h}_{i,k}$ denotes the complex conjugate of $h_{i,k}$. Since we assume the channel coefficients $h_{i,j}$ are uncorrelated and random, the expected value of $m_{i,j}$ is defined as

$$E\{m_{i,j}\} = \begin{cases} 1 & i = j \\ 0 & i \neq j. \end{cases} \tag{2.30}$$

Therefore, assuming the number of receive antennas approaches infinity, we have

$$\lim_{n_R\to\infty}\frac{\mathbf{H}^*\mathbf{H}}{n_R} = \mathbf{I} \tag{2.31}$$

where $\mathbf{I}$ denotes the $n_T \times n_T$ identity matrix. By substituting (2.31) into (2.27), we get

$$\begin{aligned} \lim_{n_R\to\infty} d^2(\mathbf{x},\mathbf{e}) &= tr\left[n_R\mathbf{B}^*(\mathbf{x},\mathbf{e})\mathbf{B}(\mathbf{x},\mathbf{e})\right] \\ &= n_R\sum_{i=1}^{n_T}\lambda_i. \end{aligned} \tag{2.32}$$

From (2.22) and (2.32), we have

$$\lim_{n_R\to\infty}\mathbf{P}(\mathbf{x}\to\mathbf{e}|\mathbf{H}) \leq \frac{1}{2}\exp\left(-n_R\frac{E_s}{4N_o}\sum_{i=1}^{n_T}\lambda_i\right). \tag{2.33}$$

This shows that as n_R approaches infinity, the channel coefficients do not have an impact on the performance. In order to minimize the pairwise probability of error, the sum of the eigenvalues of $\mathbf{A}(\mathbf{x}, \mathbf{e})$ should be maximized. This provides a code design rule when the number of receive antennas is large. Maximization of the sum of the eigenvalues of $\mathbf{A}(\mathbf{x}, \mathbf{e})$ can also be used as the design rule for finite values of n_R provided $rn_R \geq 3$ as explained in the following paragraphs.

The conditional pairwise error probability in (2.22) can also be expressed as [4]

$$P(\mathbf{x} \to \mathbf{e}|\mathbf{H}) \leq \frac{1}{2} \exp\left(-\sum_{j=1}^{n_R} \sum_{i=1}^{n_T} \lambda_i |\beta_{i,j}| \frac{E_s}{4N_o} \right) \tag{2.34}$$

where $|\beta_{i,j}|$ follows the central Chi-square distribution [13, pp. 41–44] with mean

$$\mu_{|\beta_{i,j}|^2} = 1 \tag{2.35}$$

and variance

$$\sigma^2_{|\beta_{i,j}|^2} = 1. \tag{2.36}$$

For large rn_R values, according to the central limit theorem, the expression

$$\sum_{j=1}^{n_R} \sum_{i=1}^{n_T} \lambda_i |\beta_{i,j}|^2 \tag{2.37}$$

approaches a Gaussian random variable D with mean

$$\mu_D = n_R \sum_{i=1}^{n_T} \lambda_i \tag{2.38}$$

and variance

$$\mu_D^2 = n_R \sum_{i=1}^{n_T} \lambda_i^2. \tag{2.39}$$

Thus, the unconditional pairwise error probability can be upper-bounded by

$$P(\mathbf{x} \to \mathbf{e}) \leq \int_0^{+\infty} \frac{1}{2} \exp\left(-\frac{E_s}{4N_o} D\right) p(D) dD \tag{2.40}$$

where $p(D)$ is the pdf of the Gaussian random variable D. Using

$$\int_0^{+\infty} \exp(-\gamma D) p(D) dD = \exp\left(\frac{1}{2}\gamma^2 \sigma_D^2 - \gamma \mu_D\right) Q\left(\frac{\gamma \sigma_D^2 - \mu_D}{\sigma_D}\right), \gamma > 0, \tag{2.41}$$

the upper bound in (2.40) can then be expressed as

$$P(\mathbf{x} \to \mathbf{e}) \leq \frac{1}{2} \exp\left[\frac{1}{2}\left(\frac{E_s}{4N_o}\right)^2 \sigma_D^2 - \frac{E_s}{4N_o}\mu_D\right] Q\left(\frac{\frac{E_s}{4N_o 2}\sigma_D^2 - \mu_D}{\sigma_D}\right). \tag{2.42}$$

Then by using the inequality

$$Q(x) \leq \frac{1}{2} \quad e^{x^2/2} \tag{2.43}$$

we may write

$$P(\mathbf{x} \to \mathbf{e}) \leq \frac{1}{4} \exp\left(-n_R \frac{E_s}{4N_o} \sum_{i=1}^{n_T} \lambda_i\right). \tag{2.44}$$

To minimize the pairwise error probability, $\sum_{i=1}^{n_T} \lambda_i$ must be maximized.

For a square matrix, the sum of the eigenvalues is equal to the trace of the matrix, denoted by $tr(\nu)$. It can be written as

$$tr(\nu) = \sum_{i=1}^{n_T} \lambda_i = \sum_{i=1}^{n_T} A_{i,i} \tag{2.45}$$

where $A_{i,i}$ is the ith element on the main diagonal of the matrix $\mathbf{A}(\mathbf{x}, \mathbf{e})$. Therefore, the trace of matrix $\mathbf{A}(\mathbf{x}, \mathbf{e})$ can also be expressed as

$$tr(\nu) = \sum_{i=1}^{n_T} \sum_{j=1}^{l} |e_{i,j} - x_{i,j}|^2 . \tag{2.46}$$

This shows that the trace of $\mathbf{A}(\mathbf{x}, \mathbf{e})$ is equivalent to the Euclidean distance between codewords $\mathbf{x}$ and $\mathbf{e}$ over all transmit antennas. The pairwise error probability is minimized if the Euclidean distance is maximized. When $rn_R \geq 3$, the performance of a STTC is dominated by the minimum trace of $\mathbf{A}(\mathbf{x}, \mathbf{e})$ taken over all pairs of distinct codewords $\mathbf{x}$ and $\mathbf{e}$. Therefore, a STTC designed using the trace design criterion maximize the minimum trace of $\mathbf{A(x,e)}$ over all codeword pairs [2].

2.7 STTCs Based on Trace Criterion

As mentioned in the previous section, the design criterion used for the STTCs depends on the value of rn_R. The trace criterion is applicable if $rn_R \geq 3$. For a given encoder structure, a set of coefficients is determined by minimizing the pairwise error probability. A full code search was performed over all possible pairs of paths in the code trellis by Chen *et al.* [9, 2].

The QPSK STTCs found in [2] based on the trace criterion are shown in Tables 2.2 and 2.3. It can be seen that the rank is either two or three for four transmit antennas. For three transmit antennas, the rank is also less than the number of transmit antennas. Full rank $r = n_T$ is not achievable when the trace criterion is considered. It is found in [9] that full rank is only achievable by sacrificing the maximum value of the minimum squared Euclidean distance, and vice versa. In general, codes designed using the trace criterion are effective provided $rn_R \geq 3$. The rank and determinant criteria

n_T	states	generator sequence	rank	trace
3	4	$\mathbf{g^1} = [(0,2,2),(1,2,3)]$ $\mathbf{g^2} = [(2,3,3),(2,0,2)]$	2	16.0
3	8	$\mathbf{g^1} = [(2,2,2),(2,1,1)]$ $\mathbf{g^2} = [(2,0,3),(1,2,0),(0,2,2)]$	2	20.0
3	16	$\mathbf{g^1} = [(1,2,1),(1,3,2,(3,2,1))]$ $\mathbf{g^2} = [(2,0,2),(2,2,0),(2,0,2)]$	2	24.0
3	32	$\mathbf{g^1} = [(0,2,2),(2,3,3),(1,2,2)]$ $\mathbf{g^2} = [(2,2,0),(1,2,2),(2,3,1),(2,0,0)]$	2	24.0
3	64	$\mathbf{g^1} = [(0,2,2),(3,1,0),(3,3,2),(3,2,1)]$ $\mathbf{g^2} = [(2,2,0),(2,2,2),(0,0,3),(2,0,1)]$	2	28.0

Table 2.2: QPSK STTCs with three transmit antennas based on the trace criterion [2].

have a smaller effect on the performance of STTCs when $rn_R \geq 3$.

2.8 Detection Using the Viterbi Algorithm

A STTC decoder usually uses the VA [28] to perform maximum likelihood (ML) decoding. Assuming that channel state information (CSI) is available at the receiver, the branch metrics are computed as the squared Euclidean distance between the hypothesized received symbols and the actual received signals as

$$\sum_{j=1}^{n_R} \left| r_{j,t} - \sum_{i=1}^{n_T} h_{j,i} x_{i,t} \right|^2 . \tag{2.47}$$

The VA selects the path with the minimum path metric through the code trellis.

For example, let us consider the trellis diagram of a STTC for two transmit antennas shown in Figure 2.4. The algorithm computes metrics for every

n_T	states	generator sequence	rank	trace
4	4	$\mathbf{g^1} = [(0,2,2,0),(1,2,3,2)]$ $\mathbf{g^2} = [(2,3,3,2),(2,0,2,1)]$	2	20.0
4	8	$\mathbf{g^1} = [(2,2,2,2),(2,1,1,2)]$ $\mathbf{g^2} = [(2,0,3,1),(1,2,0,3),(0,2,2,1)]$	2	26.0
4	16	$\mathbf{g^1} = [(1,2,1,1),(1,3,2,2),(3,2,1,3))]$ $\mathbf{g^2} = [(2,0,2,2),(2,2,0,0),(2,0,2,2)]$	3	32.0
4	32	$\mathbf{g^1} = [(0,2,2,2),(2,3,3,2),(1,2,2,1)]$ $\mathbf{g^2} = [(2,2,0,1),(1,2,2,0),(2,3,1,0),(2,0,0,2)]$	3	36.0
4	64	$\mathbf{g^1} = [(0,2,2,1),(3,1,0,2),(3,3,2,2),(3,2,1,3)]$ $\mathbf{g^2} = [(2,2,0,2),(2,2,2,0),(0,0,3,1),(2,0,1,2)]$	3	38.0

Table 2.3: QPSK STTCs with four transmit antennas based on the trace criterion [2].

possible path in the trellis. At each node in the trellis, the VA compares the metrics of the four paths entering the node. The path with the lowest Euclidean distance metric is retained, and the other three paths are discarded. These computations are repeated for each state in every time slot. The paths that are retained by the algorithm are called survivors or active paths. In this case, no more than four survivor paths and their metrics will be stored. The list of four paths is always guaranteed to contain the ML choice. In principle, the VA continues this process until it completes its forward search through the trellis and reaches the end of the entire data stream. In order to release decoded data to the user from time to time, trellis termination nodes are added by the receiver. The termination node is usually the all-zero state and all candidate survivor paths converge to this state. At this point, the decoder makes a decision on the ML path as only one final survivor path is retained. Then, like a block decoder, the sequence of symbols associated with that path is released as the decoded version of the received sequence.

Therefore, the VA can also be considered as a maximum likelihood sequence estimator (MLSE).

2.9 Summary

In this chapter, we have described the trellis encoder structure for multiple antenna transmission using STTCs. The number of binary information bits simultaneously fed into the trellis encoder is determined by the modulated signal constellation size M. At each symbol time, $m = \log_2 M$ information bits are processed by the STTC encoder. STTCs are typically designed such that the number of transmit antennas does not determine system throughput.

We have also summarized the upper bounds on STTC conditional pairwise error probability. System performance is dominated by the code rank r and the product of all nonzero eigenvalue of $\mathbf{A}(\mathbf{x}, \mathbf{e})$ when $rn_R \leq 3$. If full rank is achieved, it is equivalent to maximizing the minimum determinant of $\mathbf{A}(\mathbf{x}, \mathbf{e})$. Then, Bäro *et al.*'s STTCs [3] obtained according to the rank and determinant criteria should be used. On the other hand, if $rn_R \geq 3$, system performance is dominated by the minimum squared Euclidean distance between any two different codewords, or the minimum possible trace of $\mathbf{A}(\mathbf{x}, \mathbf{e})$. codes [9] should be used in this case. Some of the STTCs found in [9, 3] were listed in this chapter.

Chapter 3

STTCs for Noncoherent Communication

3.1 Introduction

The concept of a pilot sequence combined with the data symbols was developed for multiple-antenna communication on noncoherent Rayleigh fading channels by Dayal *et al.* [45]. They adopted the point of view that training may be used for noncoherent space-time block codes (STBCs) and called the resulting codes training codes [1, 45]. A similar idea was also presented by El Gamal *et al.* using what they called a threaded algebraic space-time (TAST) framework [50]. TAST is a training based signaling scheme that performs well for noncoherent communication.

In this chapter, noncoherent space-time codes (STCs) including differential STCs and training codes for noncoherent STBCs are briefly reviewed. We then revisit the concepts of noncoherent communications and introduce novel training codes for space-time trellis codes (STTCs) and noncoherent communication. We investigated the performance when two and four transmit antennas are used. Analysis shows that the performance of these noncoherent STTCs is approximately 3 dB inferior to that of coherent STTCs

when M-PSK signals are used. This result coincides with the performance gap between coherent and noncoherent communication when a single antenna is used [13].

3.2 Differential STCs for Noncoherent Communications

In most published papers [10, 51, 52, 53], differential space-time block structures are used for noncoherent communications in multiple-input multiple-output (MIMO) channel. Hughes [10] and Hochwald *et al.* [54] independently introduced a differential unitary space-time modulation (DUSTM) scheme. In DUSTM, signals are differentially transmitted block by block using unitary matrices. One of the features of DUSTM is that the signals transmitted by different antennas are mutually orthogonal as well as unitary. Detection complexity is rather low when two transmit antennas are used [55]. However, their detection suffers from an exponential complexity increase with transmitted block size [54].

As a remedy, differential space-time block codes (DSTBCs) can be employed since they utilize differential estimates and offer linear decoding complexity [56, 51]. The performance of DSTBCs is 3 dB worse than that of coherent codes with ideal channel state information (CSI) at the receiver. DSTBCs initially transmit a reference block which does not carry any data. Then the transmitter encodes the data sequence in a differential manner.

Differential modulation schemes for quasi-orthogonal space-time block codes (QOSTBC) were presented in [52]. QOSTBCs provide the full transmission rate for complex signals with three and four transmit antennas [38]. The ML decoding complexity of differential QOSTBCs and those with complete CSI increases exponentially with the number of transmit antennas [57].

There are various other differential STCs proposed in the literature [58, 59, 53]. Most of them are concatenated codes using DUSTMs or DSTBCs. A differential space-time turbo coding scheme was developed in [58]. It is a turbo code concatenated with DUSTM.

Trellis-coded modulation (TCM) for noncoherent communications based on DUSTMs was proposed in [59] when CSI is unknown to the receiver. The set partitioning approach is used to design these codes and an enlarged signal set is used. The TCM scheme is then concatenated with DUSTMs to realize differential modulation using a unitary matrix. Later in [53], differential STTCs were proposed, where STTCs are concatenated with DSTBCs. The structure of the STTC encoder within the differential STTCs of [53] is the same as the one in [2]. The encoder coefficients are optimized by code search based on the design criteria derived in [53]. The trellis encoded symbols are then mapped into DSTBC matrices for transmission. The performance of the differential STTCs is almost the same as that of the trellis-coded DUSTM over quasi-static fading channels, and is superior to that of the trellis-coded DUSTM over independent fast fading channels. The decoding complexity of the differential STTCs is lower than that of the trellis-coded DUSTM.

3.3 Training-Assisted Noncoherent STCs

Pilot-assisted modulation has been a classical engineering approach for dealing with an unknown channel [1]. For example, pilot-assisted schemes for a single transmit-receive antenna system were analyzed in [60]. In [61], training was considered for the Bell Lab's layered space-time architecture (BLAST) system of [62].

In [50], the authors proposed a training scheme which utilizes a full diversity coherent TAST block code for the noncoherent case. It outperforms

DUSTM [63]. The authors of [50] argued that using DUSTM as a *defacto* standard for noncoherent space-time communication should be reviewed. Appropriate use of coherent STCs offers a very efficient solution for noncoherent space-time communication [50].

In [1], the authors combined pilot-assisted modulation with the data symbols to create noncoherent training codes for unknown channels. They also pointed out that while training schemes have been around for a long time, people have not considered the schemes as approaches to noncoherent signal design. The training codes were thought of as a coding strategy inspired by [64]. The training codes of [1] are summarized in the following paragraphs.

To estimate the fading, the transmitted matrix $\mathbf{X}$ is split into two parts. The first part is a training sequence which is known to the receiver. The second part is the data sequence which is to be transmitted over an unknown channel. As in [1], the information matrix consists of data symbols which are encoded using a STBC so that

$$\mathbf{X} = \frac{1}{\sqrt{S}} \begin{pmatrix} \sqrt{S\tau}\mathbf{T} \\ \sqrt{1-\tau}\mathbf{Y}_1 \\ \vdots \\ \sqrt{1-\tau}\mathbf{Y}_s \end{pmatrix} \tag{3.1}$$

where the training symbols are in a $D_T \times n_T$ orthogonal matrix $\mathbf{T}$ and D_T is the training interval. The information is in S number of $D_D \times n_T$ matrices $\mathbf{Y}_i$ $(1 \leq i \leq S)$ and so that $D = D_T + SD_D$, where D is the channel coherence interval and D_D is the data transmission interval in each information matrix. Channel estimation acquired from $\mathbf{T}$ is valid within the coherence interval D. The fraction of energy spent on training for each information matrix is $\tau (0 \leq \tau \leq 1)$. The factors $\sqrt{S}$ and τ ensure that the average symbol energy of $\mathbf{X}$ is one. It is convenient to assume that the training matrix $\mathbf{T}$

has orthonormal columns [1]. It satisfies the condition

$$n_T \mathbf{T}^* \mathbf{T} = \mathbf{I}. \tag{3.2}$$

This requires a training interval of $D_T \geq n_T$ symbol intervals. In order to maximize throughput, $D_T = n_T$ should preferably be used.

The noncoherent orthogonal design in [65] can be considered as a pilot-assisted training code as discussed in [1]. When two transmit antennas are used, a training code comprising one training block and one information block transmitted over four symbol periods may be denoted as [1]

$$\frac{1}{2\sqrt{2}} \begin{pmatrix} \sqrt{2} & 0 \\ 0 & \sqrt{2} \\ x_1 & x_2 \\ -x_2^* & x_1^* \end{pmatrix} \tag{3.3}$$

where

$$x_1, x_2 = \exp\left(n \cdot \frac{2\pi j}{M}\right), \quad n = 0, 1, 2, ..., M-1 \tag{3.4}$$

are M-PSK signals and M is an integer. Similarly, we can also extend the use of training codes to STTCs. To the best of our knowledge, no published literature has investigated STTCs for noncoherent communications without the concatenation of DSTBCs or DUSTM.

In this thesis, a noncoherent STTC without the assistance of DSTBCs or DUSTM is proposed by extending the training-assisted codes of [1] to STTCs. The proposed noncoherent STTCs are less complex than the differential STTCs of [53] since no concatenation with DSTBCs is needed. The throughput loss of the proposed noncoherent STTCs compared to the differential STTCs is marginal since only a few symbols are used for training in each frame in the noncoherent STTCs. The performance gap between

the proposed noncoherent STTCs and the corresponding coherent STTCs is approximately the same as the gap between the coherent and noncoherent M-PSK using a single transmit and receive antenna. Since the differential STTCs of [53] are differentially encoded and decoded using DSTBCs, they suffer similar performance degradation as DSTBCs when compared to STBCs in a quasi-static fading channel. The proposed noncoherent STTCs provide a novel scheme for noncoherent communication without concatenation of DSTBCs or DUSTM. Meanwhile, the complexity is lower than that of differential STTCs. Therefore, the proposed noncoherent STTCs are of interest.

The design of the proposed noncoherent STTCs is the key focus of this thesis and will be discussed in Section 3.5 and Section 3.6. Before we consider noncoherent STTCs, we first revisit noncoherent modulation and demodulation.

3.4 Coherent and Noncoherent Modulation

In this section, we review the close relationships between coherent and noncoherent schemes by explaining noncoherent demodulation in coherent terms, thus breaking the dichotomy of coherent and noncoherent modulations. This also justifies Dayal *et al.* [1] and El Gamal *et al.*'s [50] treatments of using training pilots in noncoherent communications.

Consider a differential phase shift keying (DPSK) scheme with four signal points in a single-antenna system. The signal constellation can be represented by

$$\exp\left(n \cdot \frac{\pi j}{2}\right), \quad n = 0, 1, 2, 3. \tag{3.5}$$

Assume the data sequence

$$\mathbf{c} = (c_1, c_2, c_3, ..., c_t, ...) \tag{3.6}$$

is transmitted, where $c_t \in \{0, 1, 2, 3\}$. The data sequence is mapped to the signal constellation to generate a modulated symbol sequence given by

$$\mathbf{s} = (s_1, s_2, s_3, ..., s_t, ...) \tag{3.7}$$

where

$$s_t = \exp\left(c_t \cdot \frac{\pi j}{2}\right). \tag{3.8}$$

The transmitter generates the differentially modulated sequence

$$\mathbf{x} = (x_1, x_2, x_3, ..., x_t, ...) \tag{3.9}$$

where

$$\begin{aligned} x_t &= x_{t-1}s_t \\ &= x_{t-1}\exp\left(c_t \cdot \frac{\pi j}{2}\right). \end{aligned} \tag{3.10}$$

Thus, the data information is sent as the phase difference between two consecutive symbols. The initial symbol $x_0 = 1$ does not carry any information and can be thought of as a reference.

Let us represent the received data sequence by

$$\mathbf{r} = (r_1, r_2, r_3, ..., r_t, ...) \tag{3.11}$$

where

$$r_t = h_t x_t + n_t \tag{3.12}$$

is the received signal and h_t is the complex channel gain at time t. n_t is the additive white Gaussian noise (AWGN) with two sided power spectral density of $\frac{N_o}{2}$. The complex channel gain at time t is denoted h_t. The received data is processed by computing the differential phases between any two consecutive symbols. The symbol estimate is then given by

$$\begin{aligned} \hat{s}_t &= \frac{r_t}{r_{t-1}} \\ &= \frac{h_t x_t + n_t}{h_{t-1}x_{t-1} + n_{t-1}}. \end{aligned} \tag{3.13}$$

Assume that the system signal-to-noise ratio (SNR) is high, hence the noise n_t and n_{t-1} can be neglected. It is also assumed that the channel coefficient h_t is equal to h_{t-1}. Therefore, the differentially decoded phase $\hat{s}_t$ is given by

$$\hat{s}_t = \frac{x_t}{x_{t-1}} \tag{3.14}$$

where x_0 is the reference symbol. Equation (3.13) shows how DPSK is decoded at the receiver. However, the differential detection of phase can also be explained from the coherent point of view using channel estimation. Let us assume that, at time t=0, the received signal r_0 is given by

$$r_0 = h_0 x_0 + n_0 \tag{3.15}$$

where x_0 is the known reference symbol sent by the transmitter. Since the noise n_0 can be neglected at high SNR, we may write the channel estimate $\hat{h}_0$ at time $t = 0$ as

$$\hat{h}_0 = \frac{r_0}{x_0}. \tag{3.16}$$

It is assumed that the channel coefficient does not change in consecutive symbols. Therefore

$$\hat{h}_1 = \hat{h}_0 \tag{3.17}$$

where $\hat{h}_1$ is the channel estimate at time $t = 1$. The channel estimate $\hat{h}_1$ is used to decode the incoming information symbol s_1 given by

$$\begin{aligned} \hat{s}_1 &= \min_{\arg \tilde{s}_1} \left| \hat{h}_1 \tilde{s}_1 x_0 - r_1 \right|^2 \\ &= \min_{\arg \tilde{s}_1} \left| r_0 \tilde{s}_1 - r_1 \right|^2 \end{aligned} \tag{3.18}$$

where $\hat{s}_1$ is the detected information symbol and $\tilde{s}_1$ is the hypothesized information symbol at time $t = 1$. Similarly, at any arbitrary time t, channel

estimates $\hat{h}_t$ can be obtained using

$$\hat{h}_t = \hat{h}_{t-1} = \frac{r_{t-1}}{x_{t-1}} \tag{3.19}$$

where x_{t-1} is the previously transmitted symbol assumed known to the receiver. The detection of the differentially coded information symbol s_t is given by

$$\begin{aligned} \hat{s}_t &= \min_{\arg \tilde{s}_t} \left| \hat{h}_t \tilde{s}_t x_{t-1} - r_t \right|^2 \\ &= \min_{\arg \tilde{s}_t} \left| r_{t-1} \tilde{s}_t - r_t \right|^2. \end{aligned} \tag{3.20}$$

It can be seen in (3.20) that the detected symbol $\hat{s}_t$ only depends on consecutive received signals r_{t-1} and r_t. Channel estimation is done while each information symbol is detected. This process shows that differential demodulation can be explained in terms of coherent communications. This is also a reason why the DPSK scheme is also called differentially coherent modulation and demodulation [12]. However, DPSK is normally considered to be a noncoherent scheme since it does not require either perfect or explicit CSI. The imperfect or noisy CSI is implicitly conveyed by the previous symbol. This reveals the inherent link between coherent and noncoherent schemes.

3.5 Noncoherent Demodulation

3.5.1 One Transmit Antenna

Let us consider a single-antenna system transmitting a QPSK signal

$$x_t = \sqrt{\frac{2E}{T}} \cos(2\pi f_c t + \phi_t), \qquad 0 \leqslant t < T \tag{3.21}$$

where $\phi_t \in \{0, \frac{\pi}{2}, \pi, \frac{3\pi}{2}\}$, f_c is the carrier frequency, E is the signal energy per symbol and T is the symbol duration. This signal is transmitted over a channel resulting in the received signal

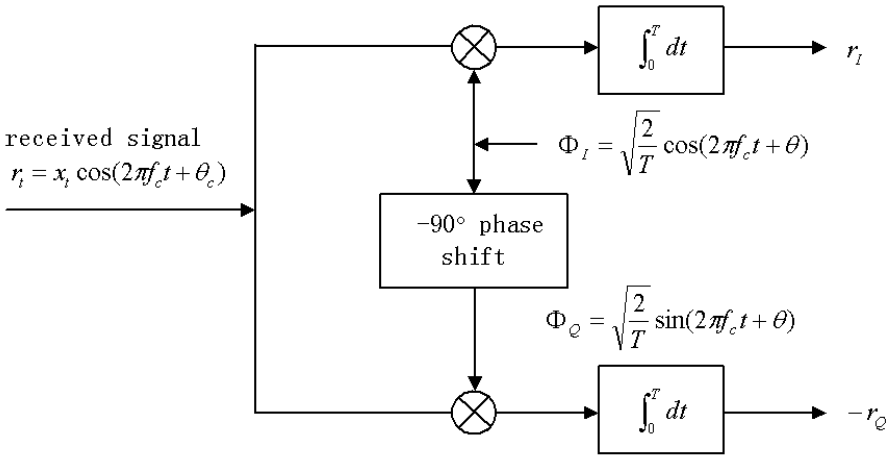

Figure 3.1: Block diagram of quadrature demodulation structure.

$$r_t = \sqrt{\frac{2E}{T}} \cos(2\pi f_c t + \phi_t + \theta_c) + n_t \tag{3.22}$$

where θ_c is the phase offset due to the channel. The phase offset θ_c is unknown to the receiver and may be considered as a random variable uniformly distributed on $[0, 2\pi)$.

We consider the noncoherent demodulation of the signal of (3.22). The signal can be decomposed into in-phase and quadrature baseband components as shown in Figure 3.1.

The received signal r_t is demodulated using the following orthogonal basis functions

$$\Phi_I = \sqrt{\frac{2}{T}} \cos(2\pi f_c t + \theta) \tag{3.23}$$

$$\Phi_Q = \sqrt{\frac{2}{T}} \sin(2\pi f_c t + \theta) \tag{3.24}$$

to produce the base band components

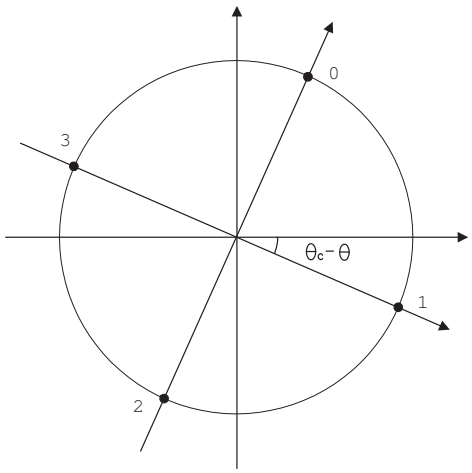

Figure 3.2: Demodulated QPSK constellation showing rotation by an unknown phase offset $(\theta_c - \theta)$.

$$r_I = \sqrt{E}\cos[\phi_t + (\theta_c - \theta)] \tag{3.25}$$

$$r_Q = \sqrt{E}\sin[\phi_t + (\theta_c - \theta)] \tag{3.26}$$

at the integrator output, where θ is an arbitrary phase. For the moment we have ignored the additive noise. This can clearly be seen to produce a rotated signal constellation, where the rotation is given by the unknown phase offset $(\theta_c - \theta)$. This is illustrated in Figure 3.2.

Now let's consider the 16-QAM signal constellation shown in Figure 3.3. In any T second signalling interval, a 16-QAM signal can be written in the form

$$x_t = \sqrt{\frac{2E}{T}}a\cos(2\pi f_c t) - \sqrt{\frac{2E}{T}}b\sin(2\pi f_c t) \qquad 0 \leqslant t < T \tag{3.27}$$

where $a, b \in \{\pm 1, \pm 3\}$. This signal can easily be written in terms of amplitude and phase or in polar form as

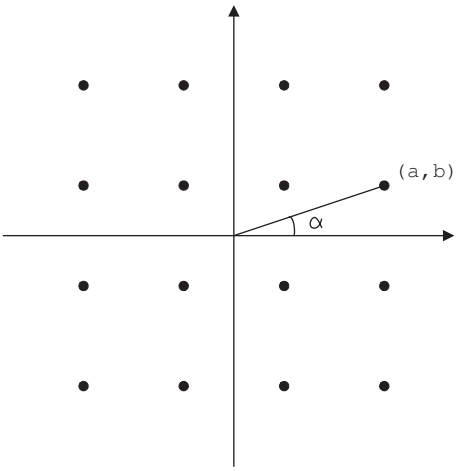

Figure 3.3: A 16-QAM constellation.

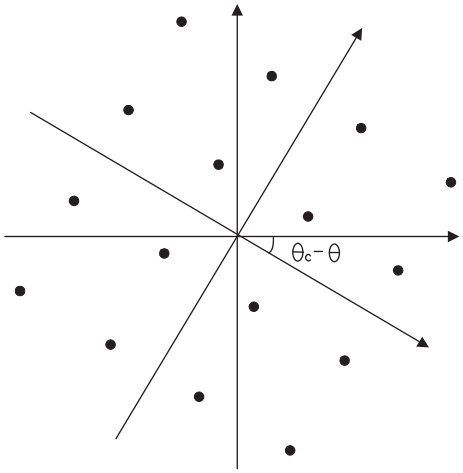

Figure 3.4: Noncoherently demodulated 16-QAM constellation showing the effect of the random phase offset ($\theta_c - \theta$).

$$x_t = \sqrt{\frac{2E}{T}}\sqrt{a^2+b^2}\cos(2\pi f_c t + \alpha) \tag{3.28}$$

where $\alpha = \tan^{-1}(\frac{a}{b})$, $a = \sqrt{a^2+b^2}\cos\alpha$, and $b = \sqrt{a^2+b^2}\sin\alpha$. After passage through the channel, the received signal can be written as

$$r_t = \sqrt{\frac{2E}{T}}\sqrt{a^2+b^2}\cos(2\pi f_c t + \alpha + \theta_c) + n_t. \tag{3.29}$$

This signal can be demodulated to obtain baseband in-phase and quadrature components using the orthogonal functions of (3.23), (3.24) and the demodulation structure of Figure 3.1 to obtain in any signalling interval

$$r_I = \sqrt{a^2+b^2}\cos\left[\alpha + (\theta_c - \theta)\right] \tag{3.30}$$

$$r_Q = -\sqrt{a^2+b^2}\sin\left[\alpha + (\theta_c - \theta)\right]. \tag{3.31}$$

These quantities lead to the rotated 16-QAM constellation shown in Figure 3.4.

At this point, we see that for any linear modulation that can be represented in complex baseband form, the resulting signal constellation will be rotated by a random phase offset consisting of the difference $(\theta_c - \theta)$ between the received signal phase and the phase of the local oscillator. In the next section, we will consider the case of noncoherent demodulation in space-time transmission.

3.5.2 Two Transmit Antennas

We now consider a space-time transmission system that employs two transmit antennas and one receive antenna as shown in Figure 3.5. For simplicity in this section, we use complex notation for all signals and channel gains.

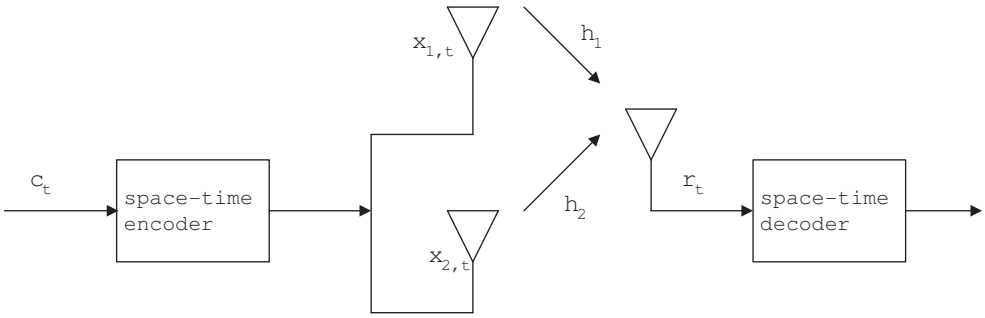

Figure 3.5: Basic block diagram of a space-time system using two transmit antennas and one receive antenna.

Since there are two transmit antennas, we need to consider two sub-channels between the transmitter and the receiver. We assume a Rayleigh flat fading channel and characterize the sub-channels by the complex gains

$$h_1 = c_1 \exp(j\theta_{c_1}) \tag{3.32}$$

$$h_2 = c_2 \exp(j\theta_{c_2}) \tag{3.33}$$

where c_1 and c_2 are Rayleigh distributed variables and the phases θ_{c_1} and θ_{c_2} are uniformly distributed random phase offsets. We may write the transmitted signals from antenna one and antenna two at time t as

$$x_{1,t} = A_1 \exp(j2\pi f_c t) \tag{3.34}$$

$$x_{2,t} = A_2 \exp(j2\pi f_c t) \tag{3.35}$$

respectively, where the complex envelopes A_1 and A_2 are chosen according to the desired modulation format. We may then write the overall received signal as

$$r_t = h_1 x_{1,t} + h_2 x_{1,t} + n_t. \tag{3.36}$$

Using (3.32), (3.33), (3.34) and (3.35), we may write the received signal as

$$r_t = c_1 A_1 \exp(j2\pi f_c t + j\theta_{c_1}) + c_2 A_2 \exp(j2\pi f_c t + j\theta_{c_2}) + n_t. \tag{3.37}$$

This signal is to be noncoherently demodulated using the receiver structure shown in Figure 3.1. In the complex domain, this is equivalent to multiplying r_t by the complex exponential $\sqrt{\frac{2E}{T}} \exp(-j2\pi f_c t - \theta)$. Neglecting the noise term for the moment, this leads to the sampled complex baseband signal at the integrator output as

$$r_t = c_1 A_1 \exp(j\theta_{c_1} - j\theta) + c_2 A_2 \exp(j\theta_{c_2} - j\theta). \tag{3.38}$$

3.5.3 Four Transmit Antennas

We now assume transmitted M-PSK signals are sent from four transmit antennas and arrive at one receive antenna via the following complex channels,

$$h_i = c_i \exp(j\theta_{c_i}), \quad i \in \{1, 2, 3, 4\} \tag{3.39}$$

where c_i is channel gain and θ_{c_i} is a random phase offset on the channel between transmit antenna i and receive antenna. The transmitted signal from the ith antenna is given by

$$x_{i,t} = A_i \exp(j2\pi f_c t) \tag{3.40}$$

where A_i is the complex envelope and $\exp(j2\pi f_c t)$ is the signal carrier with frequency f_c. The received signal at time t is the combination of four transmitted signals and can be written as

$$r_t = \sum_{i=1}^{4} h_i x_{i,t} + n_t \tag{3.41}$$

where n_t is AWGN with zero mean. In this section, we still assume the number of receive antennas n_R is equal to one. Considering the different carrier phases from each transmitter, the received signal can be written as

$$r_t = \sum_{i=1}^{4} c_i A_i \exp(j2\pi f_c t + j\theta_{c_i}) + n_t. \tag{3.42}$$

The received signal is noncoherently demodulated by multiplying (3.42) by the complex exponential $\sqrt{\frac{2E}{T}} \exp(-j2\pi f_c t + \theta)$, where θ is an arbitrary phase. Assuming noise is ignored, the base band representation of the signal after noncoherent detection is given by

$$r_t \;=\; \sum_{i=1}^{4} c_i \sqrt{E} \exp(j\theta_{c_i} - j\theta). \tag{3.43}$$

3.6 Noncoherent STTC Training Codes

3.6.1 Two Transmit Antennas

Now we introduce the proposed noncoherent STTC training codes for two transmit antennas. At the beginning of each frame of data, pilot symbols are transmitted from the two antennas. For example, if we consider the signalling format to be QPSK, and transmit the phases $(0, 0)$ from the two antennas respectively in the interval $[0, T)$, we have the transmitted signals

$$x_{1,T} = \sqrt{\frac{2E}{T}} \exp(j2\pi f_c t) \tag{3.44}$$

$$x_{2,T} = \sqrt{\frac{2E}{T}} \exp(j2\pi f_c t). \tag{3.45}$$

Similarly, if we transmit the phases $(0, \pi)$ in the interval $[T, 2T)$, we have the transmitted signals

$$x_{1,2T} = \sqrt{\frac{2E}{T}} \exp(j2\pi f_c t) \tag{3.46}$$

$$x_{2,2T} = \sqrt{\frac{2E}{T}} \exp(j2\pi f_c t + \pi). \tag{3.47}$$

Using these and (3.32), (3.33), (3.36), we obtain the sampled demodulator outputs at time T and $2T$ as

$$r_T = c_1\sqrt{E}\exp(j\theta_{c_1} - j\theta) + c_2\sqrt{E}\exp(j\theta_{c_2} - j\theta) \tag{3.48}$$

and

$$r_{2T} = c_1\sqrt{E}\exp(j\theta_{c_1} - j\theta) - c_2\sqrt{E}\exp(j\theta_{c_2} - j\theta). \tag{3.49}$$

where for the moment we have neglected any noise effects. We have also made the assumption that the fading process is either quasi-static or slowly varying, allowing us to ignore the time dependence of the fading variables. The channel coefficients thus do not change significantly between any two adjacent symbol periods. Therefore, we can use these received signals to obtain estimates of the complex fading gains as

$$\hat{h}_1 = c_1\exp(j\theta_{c_1} - j\theta) = \frac{r_T + r_{2T}}{2\sqrt{E}} \tag{3.50}$$

$$\hat{h}_2 = c_2\exp(j\theta_{c_2} - j\theta) = \frac{r_T - r_{2T}}{2\sqrt{E}}. \tag{3.51}$$

The symbol energy $\sqrt{E}$ may easily be normalized to unity in the case of M-PSK transmission. In the case of M-QAM ($M > 4$) transmission, it appears that only a constant energy modulation can be used for the pilot symbols. Therefore, complex M-QAM ($M > 4$) will not be used in this noncoherent space-time modulation scheme for training. It can, however, be used for data transmission. Coincidentally, M-QAM ($M > 4$) is not used in differential modulation/demodulation schemes in the single-antenna case either. The local oscillator phase shift θ cannot be removed since the phase differences are unknown.

Having found the channel estimates of (3.50) and (3.51), we use these to define the set of possible hypotheses in a maximum likelihood sequence estimator (MLSE) for the transmitted space-time trellis coded signal. We first construct a set of reference symbols. The members of this set will constitute a set of hypotheses for the calculation of branch metrics for the decoding of the transmitted signal using MLSE implemented via the Viterbi algorithm (VA). For the moment, we continue the example of $n_T = 2$ transmit antennas and $n_R = 1$ receive antenna that we have been using. We will discuss the four transmit antenna case in the next section. In any symbol interval, $x_{1,t}$ and $x_{2,t}$ are transmitted from the two antennas, where t represents the symbol interval index. We may then obtain the hypothesized received signal as

$$\hat{h}_1 x_{1,t} + \hat{h}_2 x_{2,t} \tag{3.52}$$

where $x_{1,t}, x_{2,t}$ range over all possible values of the modulation set. This allows the calculation of a set of branch metrics of the form

$$\left| \hat{h}_1 x_{1,t} + \hat{h}_2 x_{2,t} - r_t \right|^2 \tag{3.53}$$

where r_t is the received symbol in the symbol interval t. For an M-ary modulation, the set in (3.52) has M^2 members. ML decoding of the STTC then proceeds by means of the VA according to the trellis of the transmitted STTC.

3.6.2 Four Transmit Antennas

We now describe the noncoherent STTC training codes for four transmit antennas. The received base band signal after noncoherent detection is given by (3.43). It can be seen that the phase offset $(\theta_{c_i} - \theta)$ is unknown to the receiver. We assume that sets of pilot symbols are sent at the beginning of

each frame. The pilot symbols must be linearly independent vectors. For simplicity, the binary phase-shift keying (BPSK) signal sequence (1,1,1,1) is sent by antenna one; BPSK signal sequence (1,1,-1,-1) is sent by antenna two; BPSK signal sequence (1,-1,1,-1) is sent by antenna three and BPSK signal sequence (-1,1,1,-1) is sent by antenna four over the intervals $[0, T)$, $[T, 2T)$, $[2T, 3T)$ and $[3T, 4T)$, respectively. We may then write the equations

$$\begin{aligned} r_T &= c_1\sqrt{E}\exp(j\theta_{c_1} - j\theta) + c_2\sqrt{E}\exp(j\theta_{c_2} - j\theta) \\ &\quad + c_3\sqrt{E}\exp(j\theta_{c_3} - j\theta) - c_4\sqrt{E}\exp(j\theta_{c_4} - j\theta) \qquad (3.54) \\ r_{2T} &= c_1\sqrt{E}\exp(j\theta_{c_1} - j\theta) + c_2\sqrt{E}\exp(j\theta_{c_2} - j\theta) \\ &\quad - c_3\sqrt{E}\exp(j\theta_{c_3} - j\theta) + c_4\sqrt{E}\exp(j\theta_{c_4} - j\theta) \qquad (3.55) \\ r_{3T} &= c_1\sqrt{E}\exp(j\theta_{c_1} - j\theta) - c_2\sqrt{E}\exp(j\theta_{c_2} - j\theta) \\ &\quad + c_3\sqrt{E}\exp(j\theta_{c_3} - j\theta) + c_4\sqrt{E}\exp(j\theta_{c_4} - j\theta) \qquad (3.56) \\ r_{4T} &= c_1\sqrt{E}\exp(j\theta_{c_1} - j\theta) - c_2\sqrt{E}\exp(j\theta_{c_2} - j\theta) \\ &\quad - c_3\sqrt{E}\exp(j\theta_{c_3} - j\theta) - c_4\sqrt{E}\exp(j\theta_{c_4} - j\theta). \qquad (3.57) \end{aligned}$$

Now we assume that the noise is negligible and that the channels do not change during the periods that we are interested in. The above equations can then be solved to obtain the channel estimates

$$\begin{aligned} \hat{h}_1 &= \frac{r_T + r_{2T} + r_{3T} + r_{4T}}{4\sqrt{E}} \qquad (3.58) \\ \hat{h}_2 &= \frac{r_T + r_{2T} - r_{3T} - r_{4T}}{4\sqrt{E}} \qquad (3.59) \\ \hat{h}_3 &= \frac{r_T - r_{2T} + r_{3T} - r_{4T}}{4\sqrt{E}} \qquad (3.60) \\ \hat{h}_4 &= \frac{-r_T + r_{2T} + r_{3T} - r_{4T}}{4\sqrt{E}}. \qquad (3.61) \end{aligned}$$

We shall assume that these estimates are valid over the entire frame duration and that the symbol energy E is normalized to unity. The branch

metrics for use in VA decoding are then determined by the Euclidean distance between all possible values of the modulation set and the received signal as

$$\left| \sum_{i=1}^{4} \hat{h}_i x_{i,t} - r_t \right|^2 . \tag{3.62}$$

3.7 Performance of Noncoherent STTC Training Codes

In this section, we compute the noise variance of the received signals when they are noncoherently decoded using the channel estimation scheme of Section 3.6.

3.7.1 Two Transmit Antennas

From the branch metrics, we see that detection errors may be caused by AWGN corrupting the received signal r_t, and channel estimation noise introduced by $\hat{h}_1$ and $\hat{h}_2$. All these noises contribute to the branch metrics in (3.53). For convenience, in the performance analysis, we convert all noises into a single effective noise, which may be regarded as the AWGN added at each receiver. This effective noise can be written as

$$\tilde{n}_t = \frac{1}{2}\left(n_T + n_{2T}\right) x_{1,t} + \frac{1}{2}\left(n_T - n_{2T}\right) x_{2,t} + n_t \tag{3.63}$$

where n_T, n_{2T} and n_t are complex AWGN at time slot T, $2T$ and t respectively. They are independent zero mean complex Gaussian random variables with variance of $N_0/2$ per dimension. In base band representation, the variance of the complex noise n_t is given by

$$\sigma_{n_t}^2 = N_o. \tag{3.64}$$

The variance of the effective noise, which represents all noises, is then given by

$$\begin{aligned}\sigma^2_{\tilde{n}_t} &= E\{[\tilde{n}_t - E\{\tilde{n}_t\}]^2\} \\ &= E\Bigg\{\Bigg[\frac{1}{2}(n_T + n_{2T})x_{1,t} + \frac{1}{2}(n_T - n_{2T})x_{2,t} + n_t \\ &\quad -\frac{1}{2}E\left\{(n_T + n_{2T})x_{1,t}\right\} - \frac{1}{2}E\left\{(n_T - n_{2T})x_{2,t}\right\} \\ &\quad -E\left\{n_t\right\}\Bigg]^2\Bigg\} \qquad (3.65)\end{aligned}$$

where $E\{\cdot\}$ is the statistical expectation operator. Since n_T, n_{2T} and n_t are AWGN with zero mean, we can write

$$\begin{aligned}&\frac{1}{2}E\left\{(n_T + n_{2T})x_{1,t}\right\} \\ &= \frac{1}{2}E\left\{(n_T - n_{2T})x_{2,t}\right\} \\ &= E\left\{n_t\right\} \\ &= 0. \qquad (3.66)\end{aligned}$$

The noise variance of (3.65) becomes

$$\sigma^2_{\tilde{n}_t} = E\left\{\left[\frac{1}{2}(n_T + n_{2T})x_{1,t} + \frac{1}{2}(n_T - n_{2T})x_{2,t} + n_t\right]^2\right\} \qquad (3.67)$$

$$\begin{aligned}&= E\left\{\frac{1}{4}(n_T + n_{2T})^2(x_{1,t})^2\right\} + E\left\{\frac{1}{4}(n_T - n_{2T})^2(x_{2,t})^2\right\} \\ &\quad +E\left\{n_t^2\right\} + E\left\{\frac{1}{4}(n_T + n_{2T})(n_T - n_{2T})x_{1,t}x_{2,t}\right\} \\ &\quad +E\left\{\frac{1}{2}(n_T + n_{2T})x_{1,t}n_t\right\} + E\left\{\frac{1}{2}(n_T - n_{2T})x_{2,t}n_t\right\}. \qquad (3.68)\end{aligned}$$

Since n_t is a random sample of Gaussian processes with zero mean, we can write

$$\begin{aligned}E\{n_t^2\} &= E\{(n_t - E\{n_t\})^2\} \qquad (3.69) \\ &= \sigma^2_{n_t} \\ &= N_o\end{aligned}$$

which is the noise power. Similarly,

$$E\{n_T^2\} = N_0 \tag{3.70}$$

$$E\{n_{2T}^2\} = N_0. \tag{3.71}$$

Therefore, we can simplify the first term in (3.67) as

$$\begin{aligned} E\left\{\frac{1}{4}(n_T + n_{2T})^2(x_{1,t})^2\right\} &= E\left\{\frac{1}{4}(n_T^2 + 2n_T n_{2T} + n_{2T}^2)(x_{1,t})^2\right\} \\ &= \frac{1}{4}E\left\{n_T^2(x_{1,t})^2\right\} + \frac{1}{2}E\left\{n_T n_{2T}(x_{1,t})^2\right\} \\ &\quad + \frac{1}{4}E\left\{n_{2T}^2(x_{1,t})^2\right\} \\ &= \frac{1}{4}N_0 + 0 + \frac{1}{4}N_0 \\ &= \frac{1}{2}N_0. \end{aligned} \tag{3.72}$$

Similarly, we can write

$$E\left\{\frac{1}{4}(n_T - n_{2T})^2(x_{2,t})^2\right\} = \frac{1}{2}N_0. \tag{3.73}$$

We can find that the last three terms in (3.67) are

$$\begin{aligned} &E\left\{\frac{1}{4}(n_T + n_{2T})(n_T - n_{2T})x_{1,t}x_{2,t}\right\} \\ &= \frac{1}{4}(E\{n_T\}^2 - E\{n_{2T}\}^2)x_{1,t}x_{2,t} \\ &= 0 \end{aligned} \tag{3.74}$$

and

$$E\{(n_T + n_{2T})x_{1,t}n_t\} = 0 \tag{3.75}$$

$$E\{(n_T - n_{2T})x_{2,t}n_t\} = 0, \tag{3.76}$$

respectively. Thus (3.67) is reduced to

$$\begin{aligned} \sigma_{\tilde{n}_t}^2 &= \frac{1}{2}N_0 + \frac{1}{2}N_0 + N_0 \\ &= 2N_0. \end{aligned} \tag{3.77}$$

It can be seen that the variance of the overall noise $\tilde{n}_t$ is twice that of coherent detection when two transmit antennas and one receive antenna is used. The increase of noise is due to imperfect estimations of the CSI. From (3.77), we expect the noncoherent STTCs' performance to be approximately 3 dB inferior to coherent STTCs when two transmit antennas and one receive antenna are used. Nevertheless, the noncoherent STTCs do not need perfect channel estimation.

3.7.2 Four Transmit Antennas

When four transmit antennas are used, the possible detection error is caused by noise corrupting the received signal at time t, and channel estimation noises introduced due to errors in estimating $\hat{h}_1, \hat{h}_2, \hat{h}_3$ and $\hat{h}_4$. We convert all the noises into a single effective noise, which can be written as

$$\begin{aligned}\tilde{n}_t &= \frac{1}{4}(n_T + n_{2T} + n_{3T} + n_{4T})x_{1,t} + \frac{1}{4}(n_T + n_{2T} - n_{3T} - n_{4T})x_{2,t} \\ &\quad + \frac{1}{4}(n_T - n_{2T} + n_{3T} - n_{4T})x_{3,t} + \frac{1}{4}(-n_T + n_{2T} + n_{3T} - n_{4T}) \\ &\quad x_{4,t} + n_t \end{aligned} \tag{3.78}$$

where n_T, n_{2T}, n_{3T}, n_{4T} and n_t are independent complex Gaussian random samples at time T, $2T$, $3T$, $4T$ and t, respectively. They are zero mean with variance $N_0/2$ per dimension. The variance of the total effective noise may be written as

$$\begin{aligned}\sigma^2_{\tilde{n}_t} &= E\{[\tilde{n}_t - E\{\tilde{n}_t\}]^2\} \\ &= E\Bigg\{\Bigg[\frac{1}{4}(n_T + n_{2T} + n_{3T} + n_{4T})x_{1,t} + \frac{1}{4}(n_T + n_{2T} - n_{3T} - n_{4T})x_{2,t} \\ &\quad + \frac{1}{4}(n_T - n_{2T} + n_{3T} - n_{4T})x_{3,t} + \frac{1}{4}(-n_T + n_{2T} + n_{3T} - n_{4T})x_{4,t} + n_t\end{aligned}$$

$$-\frac{1}{4}E\{(n_T+n_{2T}+n_{3T}+n_{4T})x_{1,t}\}-\frac{1}{4}E\{(n_T+n_{2T}-n_{3T}-n_{4T})x_{2,t}\}$$
$$-\frac{1}{4}E\{(n_T-n_{2T}+n_{3T}-n_{4T})x_{3,t}\}-\frac{1}{4}E\{(-n_T+n_{2T}+n_{3T}-n_{4T})x_{4,t}\}$$
$$-E\{n_t\}\Big]^2\Big\}. \tag{3.79}$$

Since n_T, n_{2T}, n_{3T}, n_{4T} and n_t are AWGN with zero mean

$$\begin{aligned}
&\frac{1}{4}E\{(n_T+n_{2T}+n_{3T}+n_{4T})x_{1,t}\}\\
&=\frac{1}{4}E\{(n_T+n_{2T}-n_{3T}-n_{4T})x_{2,t}\}\\
&=\frac{1}{4}E\{(n_T-n_{2T}+n_{3T}-n_{4T})x_{3,t}\}\\
&=\frac{1}{4}E\{(-n_T+n_{2T}+n_{3T}-n_{4T})x_{4,t}\}\\
&=E\{n_t\}\\
&=0.
\end{aligned} \tag{3.80}$$

Therefore, we obtain

$$\begin{aligned}
\sigma^2_{\tilde{n}_t} &= E\Big\{\Big[\frac{1}{4}(n_T+n_{2T}+n_{3T}+n_{4T})x_{1,t}+\frac{1}{4}(n_T+n_{2T}-n_{3T}-n_{4T})x_{2,t}\\
&\quad+\frac{1}{4}(n_T-n_{2T}+n_{3T}-n_{4T})x_{3,t}+\frac{1}{4}(-n_T+n_{2T}+n_{3T}-n_{4T})x_{4,t}\\
&\quad+n_t\Big]^2\Big\}.
\end{aligned} \tag{3.81}$$

We further expand (3.81) as a sum of terms in an extended form as

$$\begin{aligned}
\sigma^2_{\tilde{n}_t} &= E\left\{\frac{1}{16}(n_T+n_{2T}+n_{3T}+n_{4T})^2(x_{1,t})^2\right\}\\
&\quad+E\left\{\frac{1}{16}(n_T+n_{2T}-n_{3T}-n_{4T})^2(x_{2,t})^2\right\}
\end{aligned}$$

$$
\begin{aligned}
&+E\left\{\frac{1}{16}(n_T - n_{2T} + n_{3T} - n_{4T})^2(x_{3,t})^2\right\} \\
&+E\left\{\frac{1}{16}(-n_T + n_{2T} + n_{3T} - n_{4T})^2(x_{4,t})^2\right\} + E\{n_t^2\} \\
&+E\left\{\frac{1}{8}(n_T + n_{2T} + n_{3T} + n_{4T})(n_T + n_{2T} - n_{3T} - n_{4T})x_{1,t}x_{2,t}\right\} \\
&+E\left\{\frac{1}{8}(n_T + n_{2T} + n_{3T} + n_{4T})(n_T - n_{2T} + n_{3T} - n_{4T})x_{1,t}x_{3,t}\right\} \\
&+E\left\{\frac{1}{8}(n_T + n_{2T} + n_{3T} + n_{4T})(-n_T + n_{2T} + n_{3T} - n_{4T})x_{1,t}x_{4,t}\right\} \\
&+E\left\{\frac{1}{8}(n_T + n_{2T} - n_{3T} - n_{4T})(n_T - n_{2T} + n_{3T} - n_{4T})x_{2,t}x_{3,t}\right\} \\
&+E\left\{\frac{1}{8}(n_T + n_{2T} - n_{3T} - n_{4T})(-n_T + n_{2T} + n_{3T} - n_{4T})x_{2,t}x_{4,t}\right\} \\
&+E\left\{\frac{1}{8}(n_T - n_{2T} + n_{3T} - n_{4T})(-n_T + n_{2T} + n_{3T} - n_{4T})x_{3,t}x_{4,t}\right\} \\
&+E\{(n_T + n_{2T} + n_{3T} + n_{4T})x_{1,t}n_t\} \\
&+E\{(n_T + n_{2T} - n_{3T} - n_{4T})x_{2,t}n_t\} \\
&+E\{(n_T - n_{2T} + n_{3T} - n_{4T})x_{3,t}n_t\} \\
&+E\{(-n_T + n_{2T} + n_{3T} - n_{4T})x_{4,t}n_t\}. \qquad (3.82)
\end{aligned}
$$

Assuming $n_T, n_{2T}, n_{3T}, n_{4T}$ and n_t are uncorrelated random processes, and $E\{n_T^2\} = E\{n_{2T}^2\} = E\{n_{3T}^2\} = E\{n_{4T}^2\} = E\{n_t^2\} = N_0$, we can write

$$
\begin{aligned}
&E\left\{\frac{1}{16}(n_T + n_{2T} + n_{3T} + n_{4T})^2(x_{1,t})^2\right\} \\
&= E\left\{\frac{1}{16}(n_T + n_{2T} - n_{3T} - n_{4T})^2(x_{2,t})^2\right\} \\
&= E\left\{\frac{1}{16}(n_T - n_{2T} + n_{3T} - n_{4T})^2(x_{3,t})^2\right\} \\
&= E\left\{\frac{1}{16}(-n_T + n_{2T} + n_{3T} - n_{4T})^2(x_{4,t})^2\right\} \\
&= \frac{1}{4}N_0 \qquad (3.83)
\end{aligned}
$$

and

$$\begin{aligned}
&E\left\{\frac{1}{8}(n_T+n_{2T}+n_{3T}+n_{4T})(n_T+n_{2T}-n_{3T}-n_{4T})x_{1,t}x_{2,t}\right\}\\
&=\frac{1}{8}(E\left\{n_T+n_{2T}\right\}^2-E\{n_{3T}+n_{4T}\}^2)x_{1,t}x_{2,t}\\
&=0. \qquad (3.84)
\end{aligned}$$

Similarly,

$$\begin{aligned}
&E\left\{\frac{1}{8}(n_T+n_{2T}+n_{3T}+n_{4T})(n_T-n_{2T}+n_{3T}-n_{4T})x_{1,t}x_{3,t}\right\}\\
&=E\left\{\frac{1}{8}(n_T+n_{2T}+n_{3T}+n_{4T})(-n_T+n_{2T}+n_{3T}-n_{4T})x_{1,t}x_{4,t}\right\}\\
&=E\left\{\frac{1}{8}(n_T+n_{2T}-n_{3T}-n_{4T})(n_T-n_{2T}+n_{3T}-n_{4T})x_{2,t}x_{3,t}\right\}\\
&=E\left\{\frac{1}{8}(n_T+n_{2T}-n_{3T}-n_{4T})(-n_T+n_{2T}+n_{3T}-n_{4T})x_{2,t}x_{4,t}\right\}\\
&=E\left\{\frac{1}{8}(n_T-n_{2T}+n_{3T}-n_{4T})(-n_T+n_{2T}+n_{3T}-n_{4T})x_{3,t}x_{4,t}\right\}\\
&=E\left\{(n_T+n_{2T}+n_{3T}+n_{4T})x_{1,t}n_t\right\}\\
&=E\{(n_T+n_{2T}-n_{3T}-n_{4T})x_{2,t}n_t\}\\
&=E\{(n_T-n_{2T}+n_{3T}-n_{4T})x_{3,t}n_t\}\\
&=E\{(-n_T+n_{2T}+n_{3T}-n_{4T})x_{4,t}n_t\}\\
&=0. \qquad (3.85)
\end{aligned}$$

From (3.82), (3.83), (3.84) and (3.85), we have

$$\begin{aligned}
\sigma^2_{\tilde{n}_t} &= \frac{1}{4}N_0+\frac{1}{4}N_0+\frac{1}{4}N_0+\frac{1}{4}N_0+N_0\\
&= 2N_0. \qquad (3.86)
\end{aligned}$$

Therefore, the noncoherent effective noise variance is twice that of coherent detection. Hence when four transmit antennas are used in noncoherent space-time trellis modulation, the performance is about 3 dB inferior to the coherent

demodulation case when four transmit antennas are used. This loss is due to the noisy channel estimates obtained using a limited number of pilot symbols. It is equivalent to injecting extra noise at the receiver.

Noncoherent space-time training codes and noncoherent detection for a single-antenna system show similar performance degradation compared to coherent schemes. The performance of DPSK is approximately 3 dB poorer than that for coherent M-PSK when $M \geq 4$ for a single-antenna system [13]. Note that 3 dB is only an approximate value.

3.8 Summary

This chapter has introduced the proposed training based noncoherent STTCs. A literature review of noncoherent STCs has shown that coherent STCs with the assistance of training symbols can be used for noncoherent communication with minimal modification. We showed that noncoherent decoding can be expressed in terms of coherent detection when a single transmit antenna is used. This revealed that differential detection essentially extracts CSI from the previously sent symbol. We then extended the concept of noncoherent training to STTCs by putting estimation symbols into each frame. The performance of the resulting codes is approximately 3 dB inferior to that obtained with coherent STTCs. This coincides with the performance degradation expected on noncoherent detection for a single transmit antenna.

Chapter 4

Simulation Results

4.1 Introduction

In this chapter, computer simulation results of the system proposed in Chapter 3 are presented. The main purpose is to investigate the performance of the training-assisted noncoherent STTCs presented in Chapter 3 under various conditions. The simulation environment is described in the next section. Then results are presented for noncoherent STTCs using QPSK and 8PSK modulation. Up to four transmit and four receive antennas have been used. The impact of the number of training symbols used in quasi-static flat fading channels on the system performance is investigated. All results have been obtained after at least 100 symbol or frame error events. Each data frame contains 130 M-PSK symbols from each transmit antenna including training symbols.

4.2 Simulation Environment

4.2.1 Transmitter

The binary message sequences are encoded using a STTC encoder and then transmitted from n_T antennas. The encoder outputs are mapped to complex

signal constellation points. The average symbol energy of the transmitted signal at each transmit antenna is given by

$$\sigma_s^2 = \frac{1}{n_T}. \tag{4.1}$$

Therefore, the total transmitted energy across all transmit antennas is one at each time slot. This is done to provide a fair comparison of multiple-input multiple-output (MIMO) systems with various numbers of transmit antennas. Since the total energy does not go up with the number of transmit antennas, the performance improvement from increasing the number of transmit antennas is due to increased transmit diversity.

4.2.2 Receiver

The transmitted signals are sent over a MIMO channel. It is modelled as either quasi-static or continuously varying Rayleigh fading channel. These channels are discussed in more detail in the following sections. At each receive antenna, independent additive white Gaussian noise (AWGN) is added. In reality, it is introduced by electronic components and amplifiers and is characterized as thermal noise [13].

The SNR is defined as the symbol energy to noise ratio per receive antenna. Symbol energy, E_s, is the total energy per data symbol received at each receive antenna and is the summation of energies from all transmit antennas in a multiple-antenna system. We define the total transmitted signal energy as one in each time slot. Here we define the variance of each complex channel coefficient, σ_h^2, as one. Therefore, the total symbol energy at each receive antenna is given by

$$E_s = \sigma_s^2 \sum_{i=1}^{n_T} \sigma_{h,i}^2 = 1. \tag{4.2}$$

The noise variance N_o is defined as

$$N_o = \frac{E_s}{10^{\frac{SNR}{10}}} \quad . \tag{4.3}$$

4.3 Performance over a Quasi-static Channel

4.3.1 Quasi-static Channel Model

In this thesis, wireless communication systems with n_T transmit and n_R receive antennas are considered. For a quasi-static flat Rayleigh fading channel, the channel coefficients, or elements of the $n_R \times n_T$ channel response matrix, $\mathbf{H}$, are assumed to remain unchanged during each frame. The fading gains for different frames are modelled as independent samples of complex Gaussian random variables with zero mean and a variance of 0.5 per dimension. The envelope of each channel is a Rayleigh random process.

4.3.2 One Receive Antenna

In this subsection, we compare the performances of the coherent STTC of [3] and noncoherent STTC developed in Chapter 3. We consider a system with two transmit and one receive antennas using QPSK modulation. It was explained in Chapter 2 that if the product of the code rank r ($r = n_T$ if the STTC is of full rank) and the number of receive antennas n_R is less than three, Bäro *et al.*'s STTCs [3] based on the rank and determinant criteria should be used. The STTC encoder structure is explained in Chapter 2. The four-state STTC of [3] is used in this simulation. The generator sequences are

$$\mathbf{g^1} = [(2,2),(1,0)], \tag{4.4}$$

$$\mathbf{g^2} = [(0,2),(3,1)]. \tag{4.5}$$

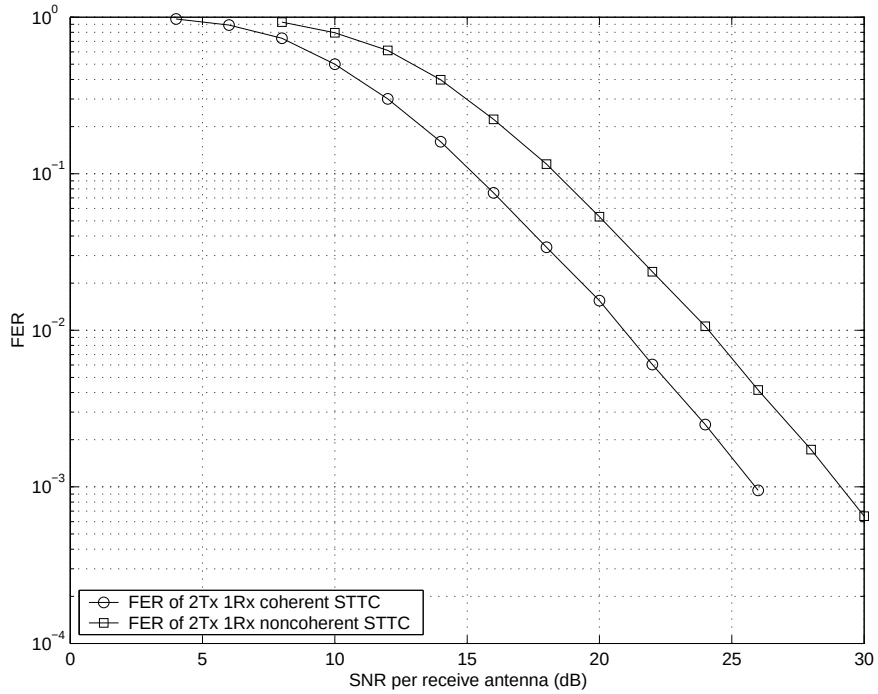

Figure 4.1: Performance of four-state coherent and noncoherent STTCs using Bäro *et al.*'s code [3], QPSK, $n_T = 2$ and $n_R = 1$.

In the simulations, each frame consists of 130 symbols from each transmit antenna including training symbols. Two training symbols were used for each antenna. There are 128 data symbols sent from each transmit antenna. The frame error rate (FER) results in Figure 4.1 show that the performance of a training-assisted noncoherent STTC is 3 dB inferior to that of the coherent STTC in a quasi-static flat fading channel at a FER of 10^{-3}. Therefore, the performance gap between the coherent and noncoherent STTCs is about the same as the gap between coherent and noncoherent M-PSK using a single transmit and receive antenna [13], namely around 3 dB. Note that in a training-assisted noncoherent STTC, the coherence time of the quasi-static

channel is assumed to be one frame.

4.3.3 Two Receive Antennas

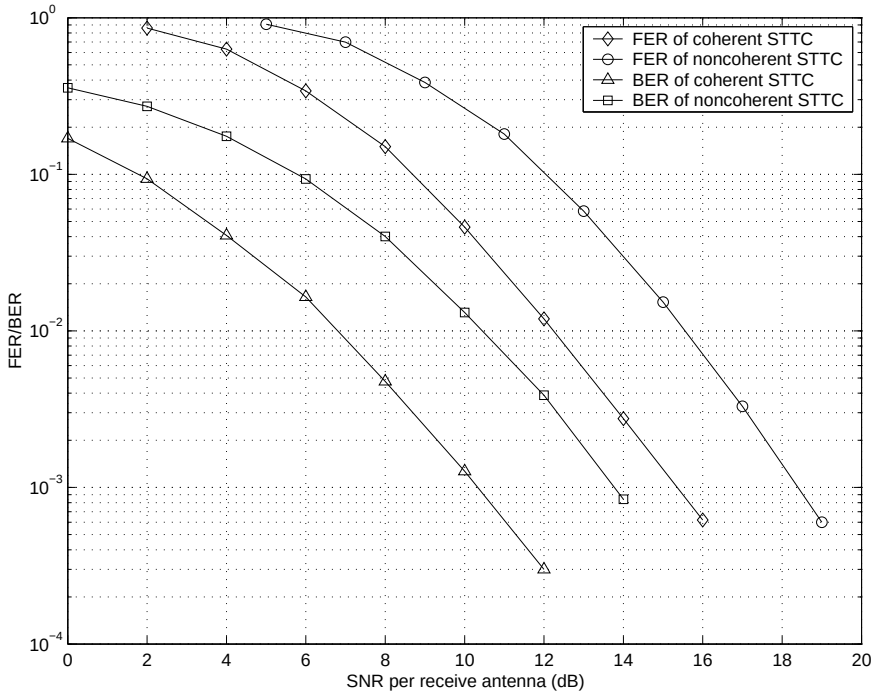

Figure 4.2: Performance of four-state coherent and noncoherent STTCs using Chen *et al.*'s code [2], QPSK, $n_T = 2$ and $n_R = 2$.

This subsection compares the performances of the coherent STTC of [2] and noncoherent STTC using two receive antennas. A system with two transmit and two receive antennas using QPSK is considered. Since the product of the code rank r and the number of receive antennas n_R is three or more, Chen *et al.*'s STTCs [2] based on the trace criterion can be used to provide maximum Euclidian distance between any erroneous and transmitted

codewords. The generator sequences are

$$\mathbf{g^1} = [(0, 2), (1, 0)], \tag{4.6}$$

$$\mathbf{g^2} = [(2, 2), (0, 1)]. \tag{4.7}$$

The frame length is 130 symbols including two training symbols for each transmit antenna. Both the bit error rate (BER) and frame error rate (FER) results are used to compare the relative performance of the coherent and noncoherent STTCs. The results in Figure 4.2 show that the performance of a noncoherent STTC using two transmit and two receive antennas is 3.1 dB inferior to that of the coherent STTC in a quasi-static flat fading channel at a FER of 10^{-3} and a BER of 10^{-3}. The FER and BER performance of a training assisted noncoherent STTC is 3.3 dB and 3.4 dB inferior to that of the coherent STTC at a FER of 10^{-2} and a BER of 10^{-2} respectively. There are 2 symbols used as training in every 130-symbol frame. The training symbols contribute 0.07 dB performance loss. Therefore, the performance gap between the coherent and noncoherent STTCs is the same as the analysis made in Section 3.7.1 when FER and BER is equal to 10^{-3}. The FER and BER performance loss of noncoherent STTCs increases when SNR decreases in this case. Similar performance gap can be observed between coherent and noncoherent M-PSK using a single transmit and receive antenna. The performance loss in differential BPSK relative to BPSK is also more significant at small SNR than the loss at large SNR [13]. It is an approximation that the performance of DPSK is 3 dB poorer than that of PSK [13].

We now consider what happens to the performance if more training symbols are sent with the noncoherent STTC in each sub-channel. Figure 4.3 shows that performance improves by 1.3 dB at a FER of 10^{-3} if four training symbols are sent when considering quasi-static flat fading channels. When eight training symbols are sent the performance improvement is around 2

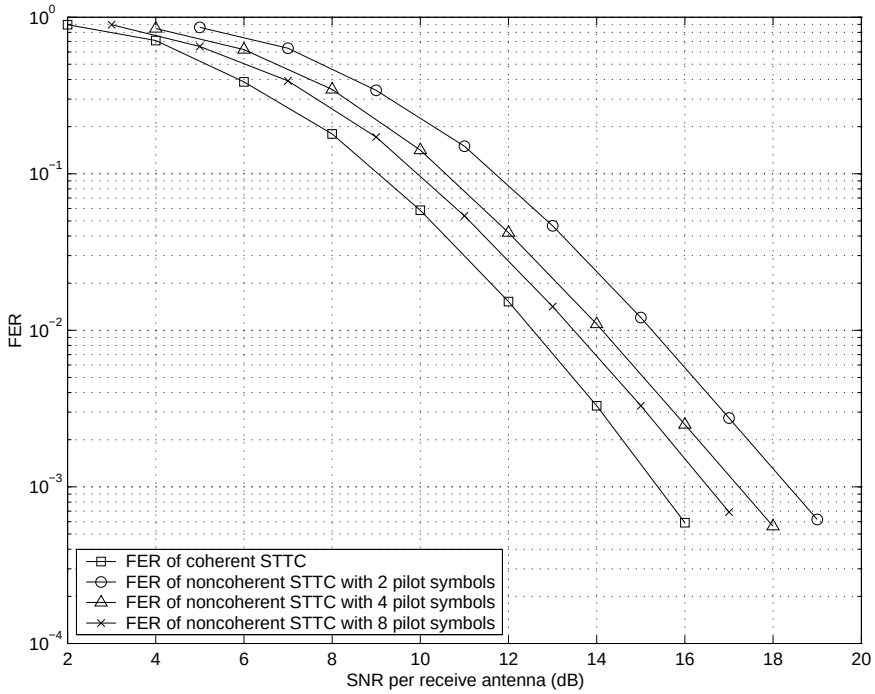

Figure 4.3: Performance of four-state coherent and noncoherent STTCs using Chen *et al.*'s code [2] with 2, 4 and 8 training symbols, QPSK, $n_T = 2$ and $n_R = 2$.

dB. This indicates that increasing the number of training symbols in the quasi-static flat fading channel can improve the system performance due to improving the quality of the channel estimates. More accurate estimation of channel coefficients $h_{i,j}$ is achieved using averaging.

Performance improvements resulting from using more training symbols are due to smaller CSI estimation errors. The estimation error depends on the number of transmit antennas and the number of training symbols. Analysis of the effective noise variance of the noncoherent STTC scheme using the minimum required number of training symbols is presented in Chapter 3. It can be seen in Figure 4.4 that the variance of the average estimation error

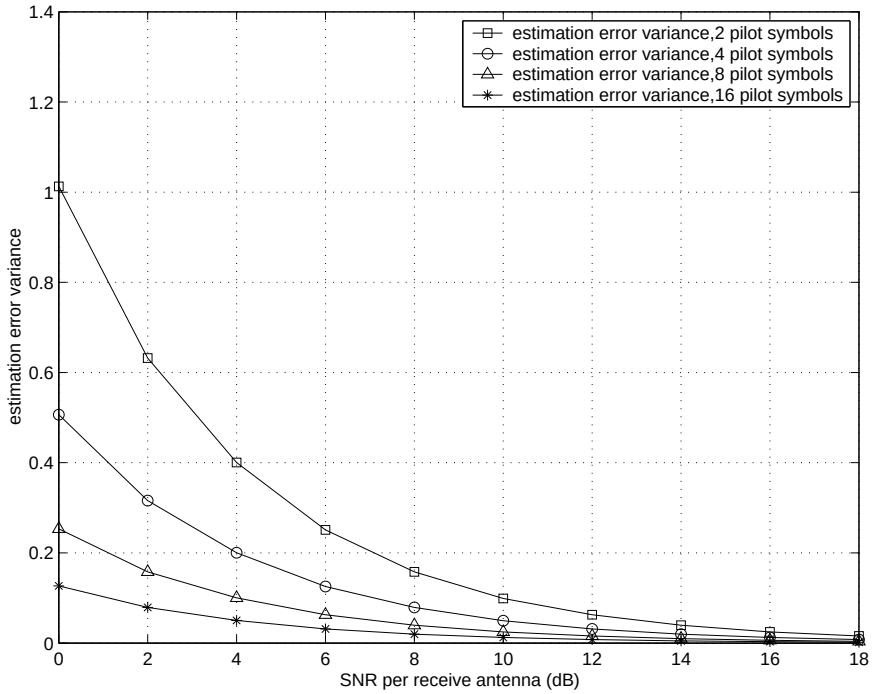

Figure 4.4: Estimation error variance, $n_T = 2$.

reduces by half when the number of training symbols is increased from 2 to 4 symbols at an SNR of 0 dB. The estimation error decreases further when the number of training symbols increases. Moreover, the estimation error due to noisy CSI also decreases when the SNR increases.

4.3.4 Four Receive Antennas

Figure 4.5 shows the performance of a coherent and noncoherent eight-state STTCs using 8PSK. Chen *et al.*'s code [9] for four transmit antennas is used. The generator sequences are

$$\mathbf{g^1} = [(2, 1, 3, 7), (3, 4, 0, 5)], \tag{4.8}$$

$$\mathbf{g^2} = [(4, 6, 2, 2), (2, 0, 4, 4)]. \tag{4.9}$$

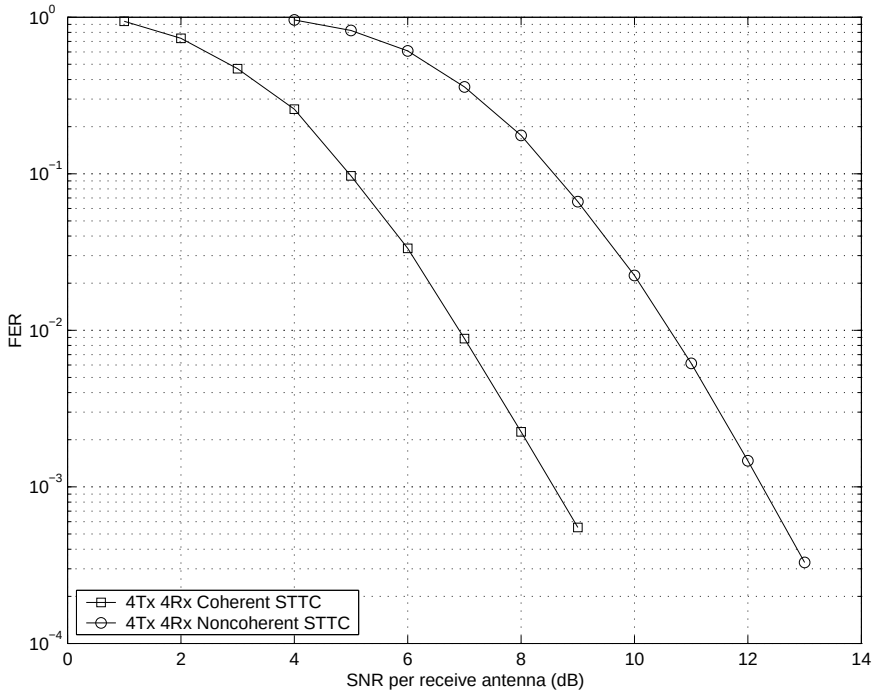

Figure 4.5: Coherent and noncoherent eight-state STTC using 8PSK, $n_T = 4$ and $n_R = 4$.

There are 130 symbols sent from each transmit antenna in each frame. Four symbols are used for training, while the remaining 126 symbols are data. FER is plotted against SNR per receive antenna in Figure 4.5. It shows that a FER of 10^{-3} can be achieved at SNR = 8.5 dB when coherent detection is used. Four training symbols are used for the noncoherent STTC and performance is 3.5 dB inferior to the coherent STTC at a FER of 10^{-3}. There is a small gap (0.5dB) between analyzed performance and simulation result in this case. This is partly due to the energy loss during training. Since four symbols are used in training in every 130 symbols, the training symbols contribute 0.14 dB performance loss.

4.4 Performance over a Continuously Varying Fading Channel

4.4.1 Rayleigh Fading Channel Model and Simulation

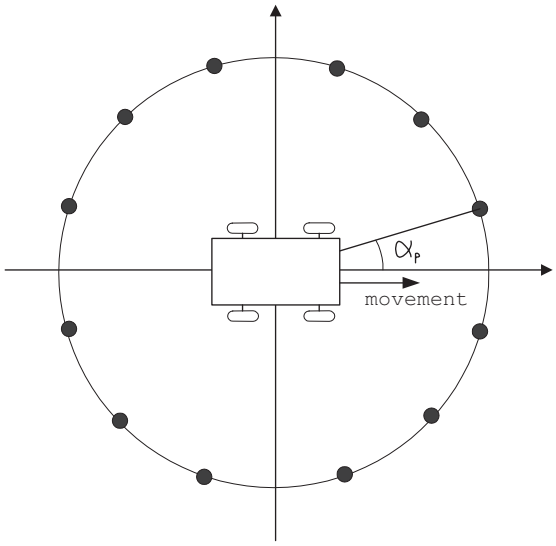

Figure 4.6: Arrival ray angles in the Jakes model.

A continuously varying Rayleigh fading channel model is applicable in most real world scenarios. A slowly varying Rayleigh fading channel is of particular interest since the CSI is highly time-correlated.

In order to investigate system performance when the mobile terminal is moving, a Rayleigh fading channel can be modelled using Clarke's fading channel model [66]. The normalized autocorrelation function of a Rayleigh fading channel with motion at a constant velocity can be modelled as a zero-order Bessel function of the first kind [66]. In Jakes' book [67], the model for Rayleigh fading based on summing sinusoids is described. This channel model was used by Jakes and others in Bell Laboratories to derive the

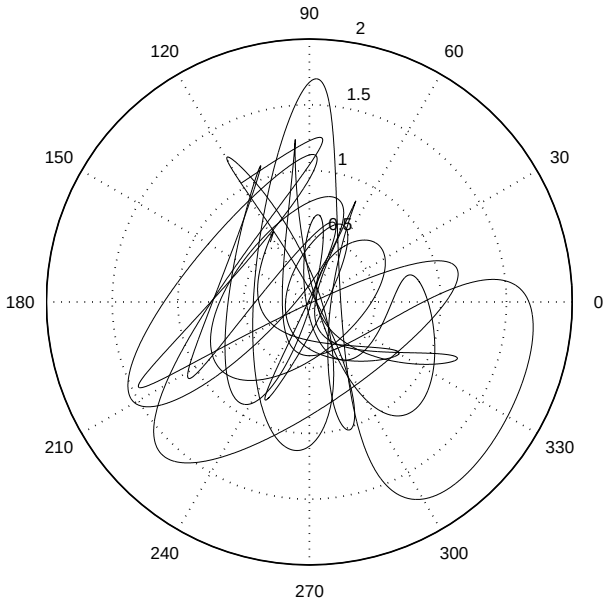

Figure 4.7: Complex Rayleigh fading with unity average channel gain plotted in polar coordinates.

comprehensive mobile radio channel model [67]. Therefore, it is also called Jakes fading model in many papers [13, 68, 69, 70, 71]. It is a deterministic method for simulating time-correlated Rayleigh fading waveforms.

Rayleigh fading of each channel coefficient is simulated by the summation of sinusoids with distinct Doppler frequencies ranging up to some maximum Doppler frequency [67]. The method assumes that P equal-strength rays arrive at a moving receiver with uniformly distributed arrival angles α_p, such that the pth ray experiences a Doppler shift $\omega_p = \omega_M cos(\alpha_p)$, where ω_M is the maximum Doppler shift. Using $\alpha_p = 2\pi(p - 0.5)/P$ in Figure 4.6, there is quadrantal symmetry in the magnitude of the Doppler shift. This leads to the model [72] for the channel response given by

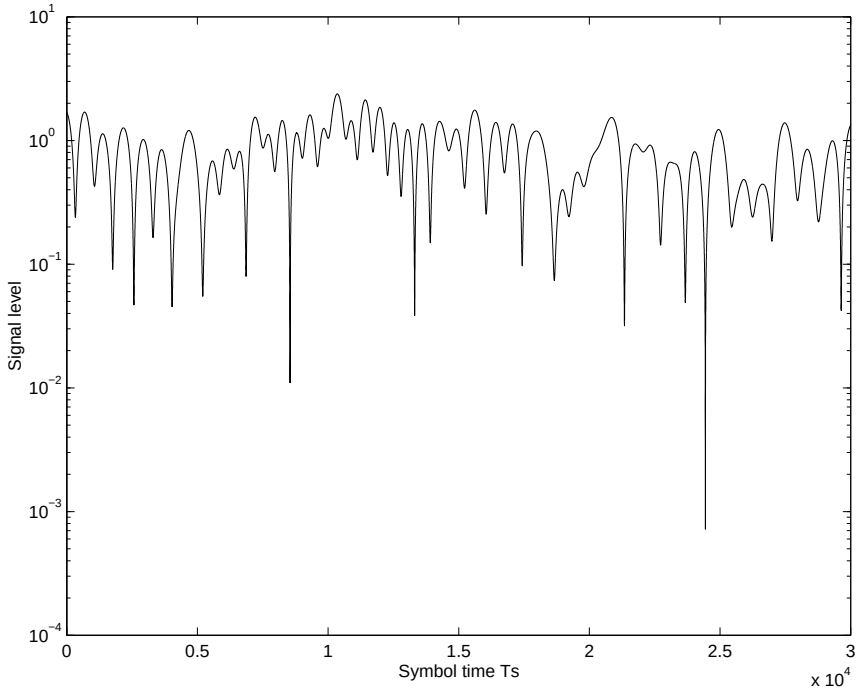

Figure 4.8: Rayleigh fading envelope.

$$h(t) = \sqrt{\frac{2}{P_o}} \sum_{p=1}^{P_o} [\cos(\beta_p) + j \sin(\beta_p)] \cos(\omega_p t + \theta_p) \tag{4.10}$$

where $P_o = P/4$ and θ_p is the initial phase, which can be randomly chosen. Setting $\beta_p = \pi p/(P_o + 1)$ gives zero cross-correlation between the real and imaginary parts of $h(t)$. If P is large enough we may invoke the central limit theorem [73] to conclude that $h(t)$ is approximately a complex Gaussian process, so that $|h|$ is Rayleigh as desired. From the work of Bennett [74] and Slack [75] it follows that the Rayleigh approximation is quite good for $P \geq 6$, with deviation from the Rayleigh distribution confined mostly to the tail of the distribution [67].

Simulations were run to generate complex baseband fading waveforms

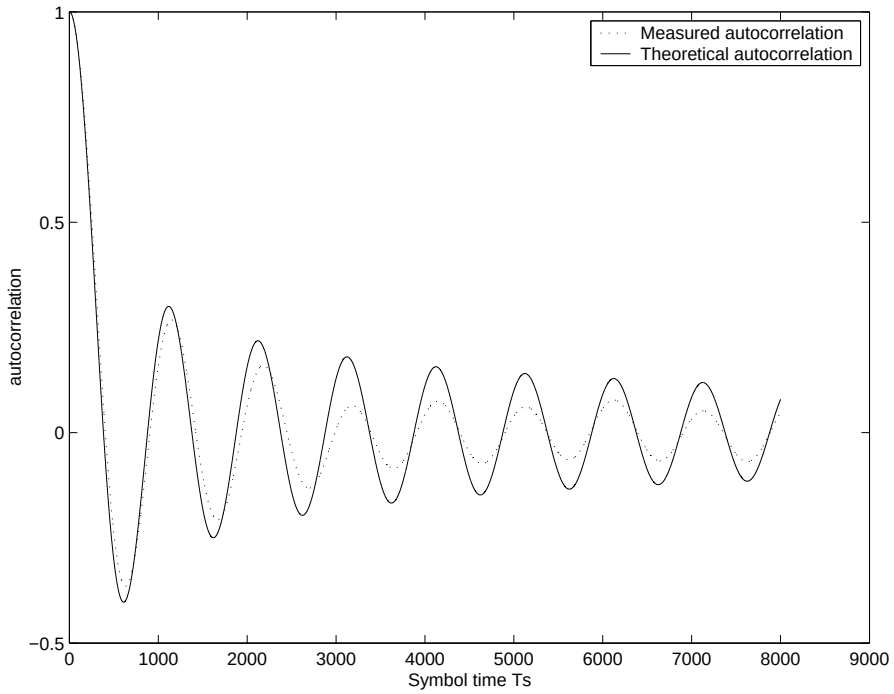

Figure 4.9: Comparison of the theoretical autocorrelation function of the fading signal with the simulation result.

to test the Rayleigh fading generator with a normalized maximum Doppler frequency $F_d = f_d T_s = 0.001$, where f_d is the maximum Doppler frequency and T_s is the symbol duration. The complex fading coefficients and fading envelope are shown in Figure 4.7 and Figure 4.8 as a function of time. It can be seen that the signal level drops as much as 10^{-3} (30 dB) during a deep fade.

The continuously varying complex fading coefficient $h(t)$ is a random process that has correlation over time. It has the temporal correlation function [76]

$$E\{h(t)h^*(t-\tau)\} = J_o(\pi f_d T_s \tau) \tag{4.11}$$

where $J_o(\cdot)$ is a Bessel function of the first kind of order zero and τ is delay.

The autocorrelation of the simulated result is plotted along with the theoretical temporal correlation of the Bessel function in Figure 4.9. The side lobes are approximately periodic in delay and their envelope decays slowly after the initial zero-crossing [68]. The agreement between theory and simulation is quite good at small to moderate values of τ, where delay, τ, is calculated by the number of symbol durations T_s.

4.4.2 Performance over a Continuously Varying Rayleigh Fading Channel

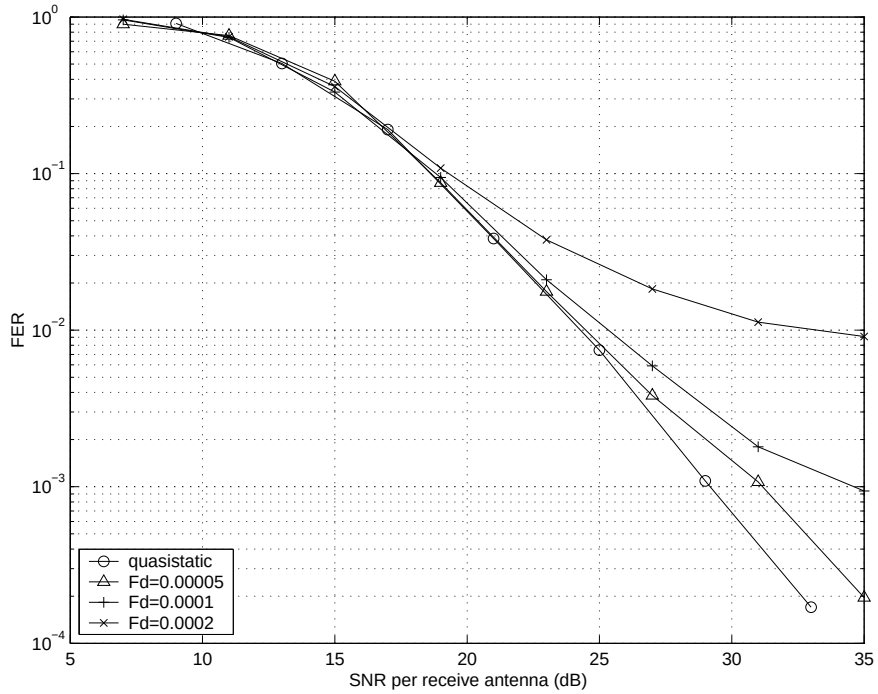

Figure 4.10: Performance of four-state QPSK STTC on the continuously varying Rayleigh fading channel for $n_T = 2$ and $n_R = 1$.

Figure 4.10 compares the simulated performance of a noncoherent STTC for various normalized Doppler frequencies. Two transmit antennas, one

receive antenna and a four-state QPSK STTC are used. A four-state Bäro *et al.*'s code [3] is used since $rn_R < 3$. The generator sequences are given by [3]

$$\mathbf{g^1} = [(2,2),(1,0)], \tag{4.12}$$

$$\mathbf{g^2} = [(0,2),(3,1)]. \tag{4.13}$$

Bäro *et al.*'s codes are based on the rank and determinant criteria. Two training symbols were sent at the beginning of each data frame. Each frame consists of 130 symbols from each transmit antenna including training symbols. It can be seen that the performance of the noncoherent STTC on a continuously fading channel is close to that on a quasi-static channel when the normalized maximum Doppler frequency is $f_dT_s = 5 \times 10^{-5}$. But performance degrades significantly at larger f_dT_s for this frame duration.

In a real system, e.g. GSM, a pilot sequence is put in the middle of each frame rather than at the beginning in order to improve the precision of the channel estimate. Figure 4.11 shows the performance of the same system when training symbols are placed in the middle of the frame instead of at the beginning of the frame. 64 data symbols (half a frame) are followed by 2 training symbols. The remaining half frame is sent after that. Each frame consists of 2 training symbols and 128 data symbols. The decoder terminates the trellis to the zero state at the end of each frame. The simulation results show improvement compared to those in Figure 4.10. The frame with a central pilot exhibits reasonable performance when $f_dT_s = 10^{-4}$. In Figure 4.11, the curve for $f_dT_s = 2 \times 10^{-4}$ shows an error floor when the FER approaches 10^{-3} instead of 10^{-2} as in Figure 4.10.

One may ask if a mobile receiver that can cope with a Doppler fading rate of $f_dT_s = 10^{-4}$ can be practically used in any real world scenarios. Let

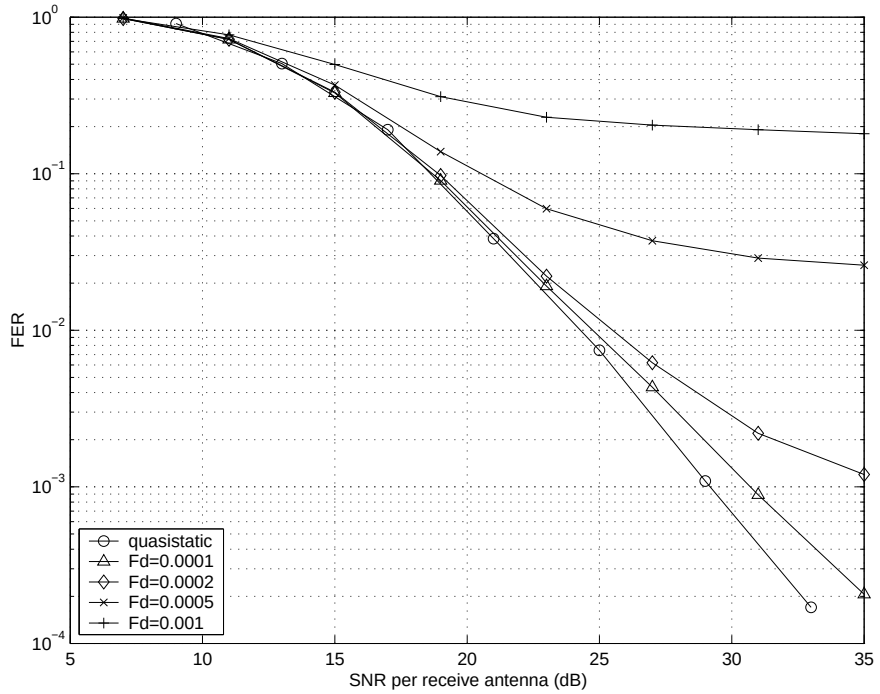

Figure 4.11: Performance of four-state QPSK STTC on continuously varying Rayleigh fading channel, $n_T = 2, n_R = 1$. Training symbols are placed in the middle of a frame.

us apply the above wireless MIMO communication system to an environment with some parameters taken from the IEEE 802.11g standard [77]. Let us assume the carrier frequency is $f_c = 2.4$ GHz, the Baud rate is $R_{Baud} = 16.5$ Msymbol/s (ERP-PBCC 33 Mbits/s formats using QPSK), and a person on a bicycle is carrying a mobile handset travelling at a speed of $v = 35$ km/hr. The normalized maximum Doppler frequency is then given by

$$\begin{aligned} f'_d T_s &= v f_c / c R_{Baud} \\ &= 4.71 \times 10^{-6} Hz \end{aligned} \tag{4.14}$$

where $c = 3 \times 10^8$ m/s is the speed of light. It can be seen that $f'_d T_s \ll 10^{-4}$ Hz. Therefore, a mobile handset carried by a fast moving person on a bicycle

in an outdoor environment sees what can be considered to be a quasi-static channel.

It can be seen that noncoherent STTCs can work well on continuously varying Rayleigh fading channels. Note that performance in terms of FER could be improved significantly by reducing the frame length.

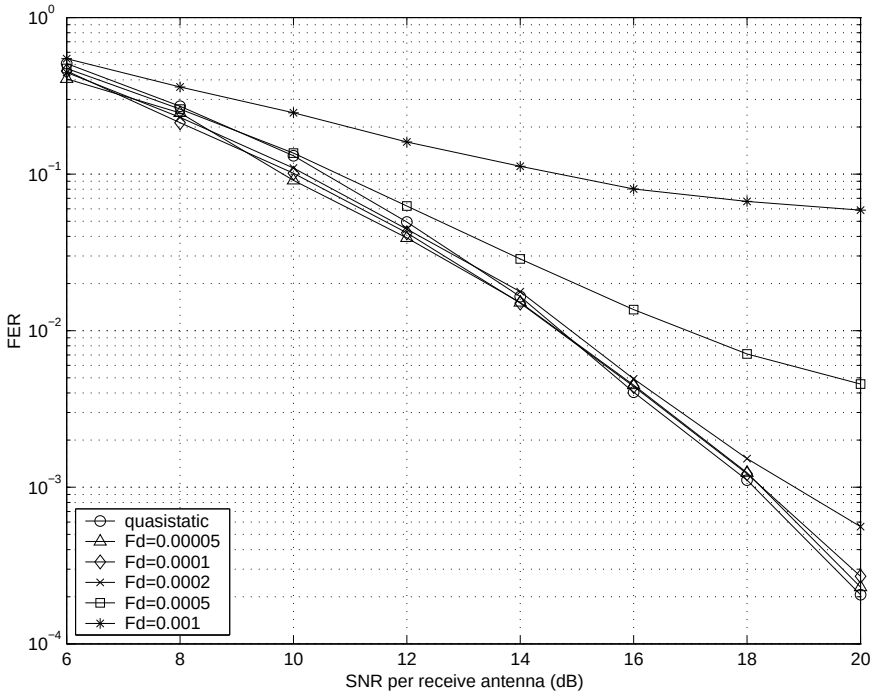

Figure 4.12: Performance of four-state QPSK STTC on continuously varying Rayleigh fading channel, $n_T = 2, n_R = 2$. Training symbols are placed in the middle of a frame.

Figure 4.12 shows the performance of the noncoherent STTC on a continuously varying Rayleigh fading channel with two transmit and two receive antennas. A four-state QPSK STTC is used. Two training symbols are placed in the middle of each frame. Since two receive antennas are used, performance is around 11 dB better than the performance when only one

receive antenna (Figure 4.11) is used at a FER of 10^{-3}. Performance is good for $f_d T_s = 10^{-4}$, but starts to deteriorate when $f_d T_s > 2 \times 10^{-4}$.

4.5 Summary

This chapter has presented simulation results for noncoherent STTCs on quasi-static and continuously time varying Rayleigh fading channels. Performance results show that a noncoherent STTC with minimum training symbols is around 3 dB inferior to a coherent STTC with perfect CSI on a quasi-static channel. Performance can be improved by sending more training symbols to reduce the estimation error variance. Noncoherent STTCs can perform well on continuously varying Rayleigh fading channels when the normalized Doppler frequency is less than or equal to 10^{-4}. Possible improvements will be discussed in the next chapter.

Chapter 5

Conclusions

This chapter presents the main contributions and findings of this thesis. Some of the important results and observations are discussed. Some suggestions for future work are discussed with a brief summary of the possible extensions to this thesis work.

5.1 Conclusions and Discussion

The thesis has developed noncoherent space-time trellis codes (STTCs) for multiple-input multiple-output (MIMO) communications. As in [1], we have adopted the point of view that "training combined with the space-time coded data symbols may be viewed as a noncoherent code".

In the first part of this thesis, we reviewed the encoder structure and decoding algorithm of STTCs. By studying the STTC design criteria and investigating an example STTC encoder, we gained an understanding of the joint design of error control coding, modulation and transmit diversity.

We then introduced the concept of using training symbols in noncoherent STTCs. By reviewing training codes for noncoherent space-time block codes (STBCs) [1] and coherent space-time codes (STCs) for noncoherent channels [50], we concluded that the combined pilot-assisted modulation with data

symbols on unknown channels can be considered as "noncoherent training codes". We then briefly summarized the training codes for noncoherent communication proposed by Dayal *et al.* in [1].

The work of [1] and other differential STCs [10, 56, 54, 51] for noncoherent communications are essentially based on STBCs. In this research, it was seen that a short sequence of training symbols can be used with STTCs for noncoherent transmission. Coincidentally, training-assisted STBCs for noncoherent MIMO communication were introduced in [1], showing that training symbols can be used with STCs as a possible solution for noncoherent MIMO communication. This thesis has further identified the fact that noncoherent STTCs with a minimum number of training symbols behave similarly to a differential detection scheme when a single transmit antenna is used in terms of performance loss due to incomplete or noisy channel state information (CSI).

We looked at the inherent relationship between coherent and noncoherent digital communication. We explained that differential demodulation of M-PSK signals can be considered as coherent demodulation through extracting CSI from previously received symbol. This justifies the treatment of using training symbols for noncoherent communications [1]. We then extended the concept of training for noncoherent communication to STTCs by using pilot symbols in each frame of the STTCs. After analyzing noncoherent STTCs for up to four transmit antennas, we concluded that the performance of noncoherent STTCs is approximately 3 dB inferior to that of coherent STTCs if the energy loss on training symbols is not considered. Therefore, the performance gap between coherent and noncoherent STTCs is approximately the same as the performance deterioration suffered by differentially detected M-PSK using a single transmit antenna. The coherence time of differentially

detected M-PSK using a single transmit antenna must be at least 2 symbol intervals since the channel state is assumed to be static over adjacent symbols. The coherence time for the quasi-static channels used by the noncoherent STTCs was assumed to be one frame.

To examine and verify the performance of the proposed noncoherent STTCs, coherent and noncoherent STTCs based on the four-state Bäro *et al.*'s code [3] using two transmit and one receive antennas were simulated. Two training symbols were transmitted from each antenna in each frame. The channel was modelled as a quasi-static flat Rayleigh fading channel. The simulation results of the training-assisted noncoherent STTCs are 3 dB inferior to that of coherent STTC when two transmit and one receive antennas are used, and when only two training intervals are used.

Similarly, coherent and noncoherent STTCs using two transmit and two receive antennas were simulated. Since the product of the code rank r and the number of receive antennas n_R is equal to or greater than three, four-state Chen et al.'s STTCs [2] based on the trace criterion are used. The simulation results show that performance gap between the noncoherent STTCs and coherent STTCs is approximately 3 dB in terms of both frame error rate (FER) and bit error rate (BER).

We also considered the performance of coherent and noncoherent STTCs using four transmit antennas and four receive antennas. Similar performance differences between them were observed.

We have noted that performance can be improved by increasing the number of training symbols used by the training-assisted noncoherent STTCs. This is due to improved channel estimates due to averaging. The error variance of the estimates reduces when the number of training symbols increases. The analysis in Chapter 3 presents the performance of noncoherent STTCs

when the minimum required number of training symbols are used.

Since continuously time varying fading channels are usually seen in real world applications, we also investigated training-assisted noncoherent STTCs in such channels. Specifically, we considered a time-varying Rayleigh flat fading channel model. We found that the performance is reasonably good when the normalized maximum Doppler frequency is less than or equal to 10^{-4} and a minimum number of training symbols are used for a noncoherent STTC with two transmit and one receive antennas. We also noted that putting training symbols in the middle of each frame improves performance in a time-varying channel.

In conclusion, this research presents training-assisted noncoherent STTCs. The emphasis of the research has been on noncoherent STTCs with a minimum number of training symbols. The noncoherent STTCs are useful when simple channel estimation is desirable in MIMO communication.

5.2 Future Work

There are a number of aspects of the current work that can be extended.

All of the current simulations are based on a frame length of 130 symbols including training symbols. By reducing the frame length, training-assisted STTCs can work on noncoherent channels when the channel coherence time (the period over which the channel state is not changing) is less than 130 symbol intervals. In some real world scenarios, it is important to be able to cope with rapidly varying channels where the channel coherence time is short. Since we already have a short training algorithm with reasonable performance, we might be able to reduce the frame length down to less than 10 symbol intervals. The penalty for this scheme is increased training overhead. By observing the performance in terms of BER, the noncoherent

STTCs with various frame lengths could be compared with each other.

Dynamic allocation of resources including transmitter power, bandwidth and bit rates based on demand is often used in modern wireless communication. For example, under the IS-95 code-division multiple access (CDMA) standard, the transmitter power of the mobiles is controlled so that the received powers at the base station is the same for all mobiles [78]. Therefore, another possible way to investigate noncoherent STTCs is to allocate an optimized fraction of energy to training symbols and data symbols while the average symbol energy remains at unity.

Appendix A

Abbreviations

Abbreviations	Definition
ADC	analog-to-digital converter
AWGN	additive white Gaussian noise
BCH	Bose-Chaudhuri-Hocquenghem
BER	bit error rate
BLAST	Bell Lab layered space-time architecture
BPSK	binary phase-shift keying
CDMA	code-division multiple access
CSI	channel state information
DAC	digital-to-analog converter
DPSK	differential phase-shift keying
DSTBC	differential space-time block codes
DUSTM	differential unitary space-time modulation
dB	decibel
det	determinant
exp	exponential
FEC	forward error correction
FER	frame error rate
GSM	global system for mobile communication

Hz	Hertz
IEEE	Institute of Electrical and Electronic Engineers
$\log_2$	logarithm to base 2
IS-95	intermediate standard-95
ITU	International Telecommunication Union
MIMO	multiple-input multiple-output
MRC	maximum ratio combining
ML	maximum likelihood
MLSE	maximum likelihood sequence estimator
PSK	phase-shift keying
QAM	quadrature amplitude modulation
QPSK	quadrature phase-shift keying
RF	radio frequency
RS	Reed-Solomon
SER	symbol error rate
SIMO	single-input multiple-output
SNR	signal-to-noise ratio
STBC	space-time block code
STC	space-time code
STTC	space-time trellis code
TCM	trellis-coded modulation
UMTS	Universal Mobile Telecommunications System
VA	Viterbi algorithm

Table A.1: Abbreviations.

Appendix B

Symbols

Symbols	Definitions
$(\cdot)^*$	transposed conjugate of
$\mathbf{A}(\mathbf{x}, \mathbf{e})$	Euclidean distance matrix of transmitted sequence $\mathbf{x}$ and received sequence $\mathbf{e}$
$\mathbf{B}(\mathbf{x}, \mathbf{e})$	difference matrix of transmitted sequence $\mathbf{x}$ and received sequence $\mathbf{e}$
$\mathbf{e}$	error vector favored by ML receiver
$E\{\cdot\}$	expected value of
E_b	average transmitted energy per bit
$e_{i,t}$	error sequence detected by ML receiver for transmit antenna i at time t
E_s	average transmitted energy per symbol
F_d	normalized Doppler frequency
f_d	Doppler frequency
$\mathbf{H}$	matrix of MIMO channel coefficient
$h_{i,j}$	channel coefficient between transmitter i and receiver j
$J_o(\cdot)$	$zero^{th}$ Bessel function of the first kind
$\mathbf{N_o}$	AWGN variance
$\mathbf{n}$	vector of received noise
$n_{j,t}$	noise at receive antenna j at time t

n_R	number of receive antennas
n_T	number of transmit antennas
P	the number of equal strength rays arriving at a moving receiver
$\mathbf{r}$	received signal vector
r	rank of the distance matrix $\mathbf{A}(\mathbf{x}, \mathbf{e})$
$r_{j,t}$	received signal at antenna j at time t
$tr(\cdot)$	trace of a matrix
T_s	symbol duration
$\mathbf{X}$	transmitted signal vector
$x_{i,t}$	transmitted STTC sequence from transmit antenna i at time t
λ_i	nonzero eigenvalues of the distance matrix $\mathbf{A}(\mathbf{x}, \mathbf{e})$
α_p	arrival angle of the p-th ray at the receiver
ω_p	doppler shift of the p-th ray at the receiver

Table B.1: Symbol definitions.

References

[1] P. Dayal, M. Brehler, and M. K. Varanasi, "Leveraging coherent space-time codes for noncoherent communication via training," *IEEE Trans. Inform. Theory*, vol. 50, no. 9, pp. 2058–2080, Sep. 2004.

[2] Z. Chen, J. Yuan, and B. Vucetic, "Improved space-time trellis coded modulation scheme on slow Rayleigh fading channels," *in Proc. IEEE ICC*, vol. 4, pp. 1110–1116, June 2001.

[3] S. Bäro, G. Bauch, and A. Hansmann, "Improved codes for space-time trellis coded modulation," *IEEE Commun. Lett.*, vol. 4, pp. 20–22, Jan. 2000.

[4] V. Tarokh, N. Seshadri, and A. Calderbank, "Space-time codes for high data rate wireless communication: Performance criterion and code construction," *IEEE Trans. Inform. Theory*, vol. 44, no. 2, pp. 744–765, Mar. 1998.

[5] S. Y. Hui and K. Y. Yeung, "Challenges in the migration to 4G mobile systems," *IEEE Commun. Mag.*, vol. 41, no. 12, pp. 54–59, Dec. 2003.

[6] "Framework and overall objectives of the future development of IMT-2000 and systems beyond IMT-2000," *ITU-R Recommendation M.1645*, June. 2003.

[7] I. Lee, C.-E. W. Sundberg, M. Sawahashi, S. Glisic, and S. McLaughlin, "Guest editorial: 4G wireless system," *IEEE J. Select. Areas Commun.*, vol. 24, no. 3, pp. 413–418, Mar. 2006.

[8] S. M. Alamouti, "A simple transmit diversity technique for wireless communication," *IEEE J. Select. Areas Commun.*, vol. 16, pp. 1451–1458, Oct. 1998.

[9] Z. Chen, B. Vucetic, J. Yuan, and K. L. Lo, "Space-time trellis codes with two, three and four transmit antennas in quasi-static flat fading channels," *in Proc. IEEE ICC*, vol. 3, pp. 1589–1595, Apr. 2002.

[10] B. Hughes, "Differential space-time modulation," *IEEE Trans. Inform. Theory*, vol. 46, no. 7, pp. 2567–2578, Nov. 2000.

[11] G. J. Foschini and M. J. Gans, "On limits of wireless communication in a fading environment when using multiple antennas," *Wireless Personal Commun.*, vol. 6, no. 3, pp. 311–335, Mar. 1998.

[12] S. Haykin, *Communication Systems, 4th ed.* New York: John Wiley & Sons, 2001.

[13] J. G. Proakis, *Digital Communications, 4th ed.* New York: McGraw-Hill, 2001.

[14] C. E. Shannon, "Communication in the presence of noise," *in Proc. IRE*, vol. 37, no. 1, pp. 10–21, Jan. 1949.

[15] R. Hamming, "Error detecting and error correcting codes," *Bell Syst. Tech. J.*, vol. 29, pp. 147–160, 1950.

[16] A. Hocquenghem, "Codes correcteurs d'erreurs," *Chiffres*, vol. 2, pp. 147–156, Sep. 1959.

[17] R. Bose and D. Ray-Chaudhuri, "On a class of error-correcting binary group codes," *Inform. Control*, vol. 3, pp. 68–79, Mar. 1960.

[18] ——, "Further results on error correcting binary group codes," *Inform. Control*, vol. 3, pp. 279–290, Sep. 1960.

[19] W. Peterson, "Encoding and error-correction procedures for the Bose-Chaudhuri-Hocquenghem codes," *IRE Trans. Inform. Theory*, vol. 6, pp. 459–470, Sep. 1960.

[20] I. Reed and G. Solomon, "Polynomial codes over certain finite fields," *J. Soc. Ind. Appl. Math.*, vol. 8, pp. 300–304, June 1960.

[21] *Recommendations for Space Data System Standards: Telemetry Channel Coding.* Reston, Virginia: Consultative Committee for Space Data Systems, May 1984.

[22] P. Elias, "Coding for noisy channels," *in IRE Nat. Conv. Rec.*, pp. 37–47, 1955.

[23] J.Wozencraft, "Sequential decoding for reliable communication," *in IRE Nat. Conv. Rec.*, vol. 5, no. 2, pp. 11–25, 1957.

[24] J. Wozencraft and B. Reiffen, *Sequential Decoding.* Cambridge, MA: MIT Press, 1961.

[25] R. Fano, "A heuristic discussion of probabilistic coding," *IEEE Trans. Inform. Theory*, vol. 9, pp. 64–74, Apr. 1963.

[26] J. Massey, *Threshold Decoding.* Cambridge, MA: MIT Press, 1963.

[27] A. Viterbi, "Error bounds for convolutional codes and an asymptotically optimum decoding algorithm," *IEEE Trans. Inform. Theory*, vol. 13, pp. 260–269, Apr. 1967.

[28] G. D. Forney, "The Viterbi algorithm," *in Proc. IEEE*, vol. 61, no. 3, pp. 268–278, Mar. 1973.

[29] J. Heller and I. Jacobs, "Viterbi decoding for satellite and space communication," *IEEE Trans. Commun. Technol.*, vol. 19, pp. 835–848, Oct. 1971.

[30] G. Ungerboeck, "Channel coding with multilevel/phase signals," *IEEE Trans. Inform. Theory*, vol. IT-28, pp. 55–67, Jan. 1982.

[31] ——, "Trellis-coded modulation with redundant signal sets-Part I: Introduction," *IEEE Commun. Mag.*, vol. 25, pp. 5–11, Feb. 1987.

[32] C. Berrou, A. Glavieux, and P. Thitimajshima, "Near shannon limit error-correcting coding and decoding: Turbo codes," *in Proc. IEEE ICC*, pp. 1064–1070, Geneva, Switzerland, May 1993.

[33] B. Glance and L. Greestein, "Frequency-selective fading effects in digital mobile radio with diversity combining," *IEEE Trans. Commun.*, vol. 31, no. 9, pp. 1085–1094, Sep. 1983.

[34] F. Adachi and K. Ohno, "BER performance of QDPSK with postdetection diversity reception in mobile radio channels," *IEEE Trans. Veh. Technol.*, vol. 40, no. 1, pp. 237–249, Feb. 1991.

[35] H. Zhou, R. Deng, and T. Tjhung, "Performance of combined diversity reception and convolutional coding for QDPSK land mobile radio," *IEEE Trans. Veh. Technol.*, vol. 43, pp. 499–508, Aug. 1994.

[36] V. Tarokh, H. Jafarkhani, and A. Calderbank, "Space-time block codes from orthogonal designs," *IEEE Trans. Inform. Theory*, vol. 45, pp. 1456–1467, July 1999.

[37] A. Lozano, A. Goldsmith, R. A. Valenzuela, M. A. Lagunas, and D. Gesbert, "Advances in smart antennas," *IEEE Wireless Commun.*, vol. 13, no. 4, pp. 6–30, Aug. 2006.

[38] H. A. Jafarkhani, "A quasi-orthogonal space-time block code," *in Proc. IEEE WCNC*, vol. 1, pp. 23–28, Sep. 2000.

[39] T. H. Liew and L. Hanzo, "Space-time codes and concatenated channel codes for wireless communications," *in Proc. IEEE*, vol. 90, no. 2, pp. 187–219, Feb. 2002.

[40] Z. Chen, B. Vucetic, and J. Yuan, "Space-time trellis codes with transmit antenna selection," *Electron. Lett.*, vol. 39, no. 11, pp. 854–855, May 2003.

[41] E. I. Telatar, "Capacity of multi-antenna Gaussian channels," *AT&T Bell Labs. Intern. Tech. Memo.*, June 1995.

[42] ——, "Capacity of multi-antenna Gaussian channels," *Europ. Trans. Telecom.*, vol. 10, pp. 585–595, Nov. 1999.

[43] C. E. Shannon, "A mathematical theory of communicaiton," *Bell Syst. Tech. J.*, vol. 27, pp. 379–423, July 1948.

[44] ——, "A mathematical theory of communicaiton," *Bell Syst. Tech. J.*, vol. 27, pp. 623–656, Oct. 1948.

[45] M. Brehler and M. K. Varanasi, "Training-codes for the noncoherent multi-antenna block-Rayleigh-fading channel," *in Proc. Conf. Inform. Sciences and Syst.*, Baltimore, MD, Mar. 2003.

[46] M. Tao and R. S. Cheng, "Improved design criteria and new trellis codes for space-time coded modulation in slow flat fading channels," *IEEE Commun. Lett.*, vol. 5, pp. 313–315, July 2001.

[47] J. Yuan, B. Vucetic, Z.Chen, and W.Firmanto, "Performance of space-time coding on fading channels," *in Proc. ISIT*, June 2001.

[48] S. B. Wicker, *Chapter 14. Trellis Coded Modulation, Error Control Systems for Digital Communication and Storage.* Upper Saddle River, New Jersey: Prentice Hall, 1995.

[49] D. C. Lay, *Linear Algebra and Its Applications, 2nd ed.* Addison Wesley, 1997.

[50] H. El Gamal, D. Aktas, and M. O. Damen, "Coherent space-time codes for noncoherent channels," *in Proc. GLOBECOM*, vol. 4, pp. 1915–1919, Dec. 2003.

[51] H. Jafarkhani and V. Tarokh, "Multiple transmit antenna differential detection from generalized orthogonal designs," *IEEE Trans. Inform. Theory*, vol. 47, pp. 2626–2631, Sep. 2001.

[52] Y. Zhu and H. A. Jafarkhani, "Differential modulation based on quasi-orthogonal codes," *IEEE Trans. Wireless Commun.*, vol. 4, pp. 3005–3017, Nov. 2005.

[53] Y. Li and B. Vucetic, "Design of differential space-time trellis codes," *IEEE Trans. Wireless Commun.*, vol. 6, no. 5, pp. 1631–1637, May 2007.

[54] B. M. Hochwald and T. L. Marzetta, "Unitary space-time modulation for multiple-antenna communications in Rayleigh flat fading," *IEEE Trans. Inform. Theory*, vol. 46, pp. 543–564, Mar. 2000.

[55] B. Allen, Y. Kuroda, F. Said, and A. Aghvami, "Performance of differential and differential unitary space-time block codes over spatially correlated Rayleigh fading channels," *in Proc. IEE Conf. 3G Mobile Commun. Technol.*, pp. 378–382, 2004.

[56] V. Tarokh and H. H. Jafarkhani, "A differential detection scheme for transmit diversity," *IEEE J. Select. Areas Commun.*, vol. 18, no. 7, pp. 1169–1174, July 2000.

[57] A. Y. Peng, I. Kim, and S. Yousefi, "Low-complexity sphere decoding algorithm for quasi-orthogonal space-time block codes," *IEEE Trans. Commun.*, vol. 54, no. 3, pp. 377–382, Mar. 2006.

[58] C. Schlegel and A. Grant, "Differential space-time turbo codes," *IEEE Trans. Inform. Theory*, vol. 49, no. 9, pp. 2298–2306, May 2003.

[59] M. Tao and R. S. Cheng, "Trellis-coded differential unitary space-time modulation over flat fading channels," *IEEE Trans. Commun.*, vol. 51, no. 4, pp. 587–596, Apr. 2003.

[60] J. K. Cavers, "An analysis of pilot symbol assisted modulation for Rayleigh fading channels," *IEEE Trans. Veh. Technol.*, vol. 40, pp. 686–693, Nov. 1991.

[61] T. L. Marzetta, "BLAST training: Estimating channel characteristics for high capacity space-time wireless," *in Proc. Allerton Conf. Communications, Control and Computing*, vol. 1, no. 2, pp. 41–59, Monticello, IL, Sep. 1999.

[62] G. J. Foschini, "Layered space-time architecture for wireless communication in fading environments when using multiple antennas," *Bell Labs. Tech. J.*, vol. 1, no. 2, pp. 41–59, 1996.

[63] Y. Jing and B. Hassibi, "Unitary space-time modulation via Cayley transform," *IEEE Trans. Signal Processing*, vol. 51, pp. 2891–2904, Nov. 2003.

[64] B. Hassibi and B. M. Hochwald, "How much training is needed in multiple-antenna wireless links?" *IEEE Trans. Inform. Theory*, vol. 49, pp. 951–963, Apr. 2003.

[65] V. Tarokh and I.-M. Kim, "Existence and construction of noncoherent unitary space-time codes," *IEEE Trans. Inform. Theory*, vol. 48, no. 12, pp. 3112–3117, Dec. 2002.

[66] R. H. Clarke, "A statistical theory of mobile-radio reception," *Bell Syst. Tech. J.*, vol. 47, pp. 957–1000, July 1968.

[67] W. C. Jakes, *Microwave Mobile Communications.* New York: John Wiley & Sons, 1974.

[68] W. Transter, K. Shanmugan, T. S. Rappaport, and K. L. Kosbar, *Principles of Communication Systems Simulation with Wireless Applications.* Upper Saddle River, New Jersey: Prentice Hall, 2004.

[69] R. D. Koilpillai, S. Channakeshu, and R. L. Toy, "Low complexity equalizers for US Digital Cellular System," *in Proc. VTC*, vol. 2, pp. 744–747, May 1992.

[70] N. W. K. Lo, D. D. Falconer, and A. U. H. Sheikh, "Adaptive equalization and diversity combining for mobile radio using interpolated channel

estimates," *IEEE Trans. Veh. Technol.*, vol. 40, no. 3, pp. 636–645, Aug. 1991.

[71] G. L. Stuber and L.-B. Yiin, "Downlink outage predictions for cellular radio systems," *IEEE Trans. Veh. Technol.*, vol. 40, no. 3, pp. 521–531, Aug. 1991.

[72] P. Dent, G. E. Bottomley, and T. Croft, "Jakes fading model revisited," *Electron. Lett.*, vol. 29, no. 13, pp. 1162–1163, June 1993.

[73] H. Stark and J. W. Wood, *Probability and Random Process with Application to Signal Processing, 3rd ed.* Upper Saddle River, New Jersey: Prentice Hall, 2002.

[74] W. R. Bennett, "Distribution of the sum of randomly phased components," *Quart. Appl. Math.*, pp. 385–393, Jan. 1948.

[75] M. Slack, "The probability distributions of sinusoidal oscillations combined in random phases," *J. Inst. Elec. Eng.*, vol. 93, no. 3, pp. 76–86, 1946.

[76] T. S. Rappaport, *Wireless Communications: Principles and Practice, 2nd ed.* Upper Saddle River, New Jersey: Prentice Hall, 2002.

[77] IEEE Computer Society, "Telecommunications and information exchange between systems - Local and metropolitan area networks - Specific requirements, part 11: Wireless LAN medium access control (MAC) and physical layer (PHY) specifications, amendment 4: Further higher data rate extension in the 2.4 GHz band," *IEEE Std 802.11g, IEEE Standard for Information Technology*, June 2003.

[78] D. N. C. Tse and S. V. Hanly, "Multiaccess fading channels-Part I: Polymatroid structure, optimal resource allocation and throughput capacity," *IEEE Trans. Inform. Theory*, vol. 44, no. 7, pp. 2796–2815, Nov. 1998.